Responses to Review Comments on HESS-2020-43-R1

We thank the anonymous referee #3 for the comments and suggestions. We have addressed the comments point-by-point in the revision. In the text below, comments are repeated verbatim and the corresponding responses are in blue. Also, we have made substantial improvements to the manuscript based on the comments and suggestions, and the label lines in brackets below are based on the clean version of the revised manuscript.

Anonymous Referee #3

Authors have included some of my comments in the revised version of the manuscript. However, it is clear that Authors are resisting to look at some of the comments which actually raise serious objections on the efficacy of the proposed two-steps blending approach and consequently the validation of results. In the previous version also, I had commented that details were not provided on many critical aspects. Authors have admitted the limitations of the previous version of the manuscript. Now in the revised version, they have somehow tried to satisfy my comments by adding more analysis but again the presented details in the methodology are hardly sufficient. In summary, I feel resistant from Authors to perform any further investigation about their approach, analysis with more years of data and provide more details on the parameter estimation using a dataset. In my view, the revised manuscript tries to demonstrate a potential approach with lack of in-depth analysis. I would recommend major revision.

Response: We appreciate the reviewer for the critical comments. In this revision, the approach is further investigated and clarified as required by this reviewer. Also, we perform more years of data in the warm season of 2010 to 2014 for model validation and provides more details of parameter estimation. Detailed information can be found in the following point-by-point responses and the revised manuscript.

Authors may want to work on my following comments:

[1] Section 3.2 says “The goodness-of-fit of the Student’s t distribution for the bias between GR and SPE is examined graphically by using a quantile-quantile plot at the training sets (Fig. 3). It is found that they are close to the diagonal red line.” Please look at Figure 3, the distribution is

completely skewed. Blue dots are hardly lying on the diagonal red line. If the distribution is not properly set, then the parameter estimation and results will have errors.

Response: We thank the reviewer for the important comment. We have fixed the mistake in the revised version. Student distribution is a symmetric distribution, which is therefore not suitable for skewed data. To find a suitable distribution, we tested several distributions including Lognormal, Gaussian (just for comparison) and Gamma distribution. It is found that a Gamma distribution is more appropriate as its Probability-Probability (PP) plots are closer to the diagonal black line for the training data in the warm season of 2014 in the northeast Tibetan Plateau (Figure 3). In the revision, a Gamma distribution is replaced in the first stage. We have also rephrased the related expression in the revised manuscript as pointed out by this reviewer (Lines 107-111).

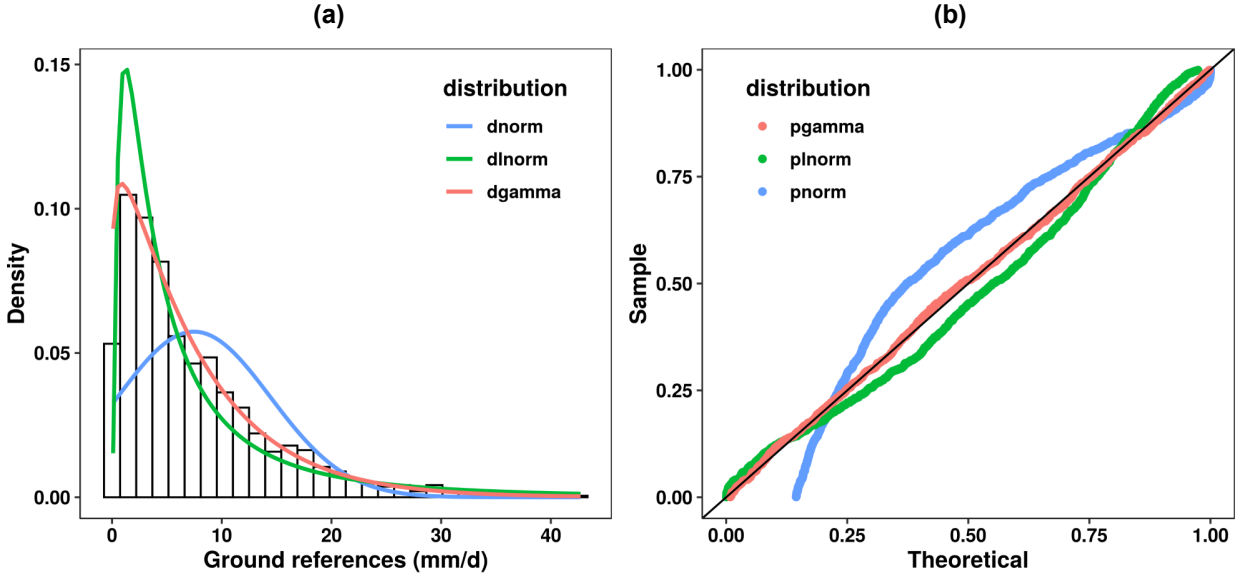

Figure 3: (a) The histogram density plot and (b) the corresponding Probability-Probability plot of GR at the training grids in the warm season of 2014 in the NETP, where the red, blue and green lines shows the fitted Gamma, Lognormal and Gaussian distribution, respectively..

Regarding the estimation of parameters, please look at Robertson et al. 2013, 'Post-processing rainfall forecasts from numerical weather prediction models for short-term streamflow forecasting' where MCMC approach of estimating parameters were changed to MAP approach based on the available length of data. Also please look at the parameter estimation section in Shrestha et al. 2015, 'Improving Precipitation Forecasts by Generating Ensembles through Postprocessing.' This is one of the reasons why I had requested Authors to explain the steps to estimate parameters using

some example dataset. It seems that Authors are hesitating to present this in the manuscript. Instead, Authors have added few more equations in the methodology section to make it appear more descriptive.

Response: We appreciate for the reviewer's suggestion, especially the two papers. We have added the two references in the revised manuscript. We also agree that accurate parameter information is fundamental for model inference as pointed out by this reviewer.

In the revised manuscript, the Markov Chain Monte Carlo (MCMC) technique with its sampling algorithm as the No-U-Turn Sampler (NUTS) variant of Hamiltonian Monte Carlo in the Stan program is performed to address this issue. The sampling records of model parameters are obtained based on the training data in the warm season of 2014 in the NETP. Since we only have four parameters in this model, the MCMC converges very quickly. Thus, we run a chain of length 2000, removing the first 1000 iterations as the warm-up period and retaining the second 1000 iterations. The parameter samples of these 1000 iterations are the samples of the posterior distribution $f(\boldsymbol{\theta}_i|\mathbf{R}, \boldsymbol{Y}_i, \boldsymbol{Z})$. The prediction of bias-corrected SPE in Stage 1 is performed using the MCMC iterated samplings. As for each SPE, a numerical algorithm is suggested based on the replicate of the post-convergence MCMC samples. The mean value of the MCMC samples R_k^*, denoted by Y_i', is regarded as the bias-corrected SPE and the associated credible intervals (e.g., 2.5% and 97.5% quantiles) is used for predictive uncertainty. In Step 2, the estimation process in a Bayesian framework is similar to that described in Stage 1. After all parameters are estimated, as similar to the Bayesian inference in Stage 1, the blended SPE at any site and time can be derived with the bias-corrected SPE and corresponding weights using the MCMC iterations.

In the revised manuscript, the TSB model structure, parameter estimation and Bayesian inference are reorganized in "*Section 3.1 TSB"* of the "*Methodology*" part (Lines 94-185). In addition, the parameter estimates are analyzed in "*Section 4.1 Parameter estimates"* of the "*Result*" part (Lines 226-237), where Figures 4 and 5 shown below are the PDF curves of posterior parameter sets in the bias-correction and data merging stages.

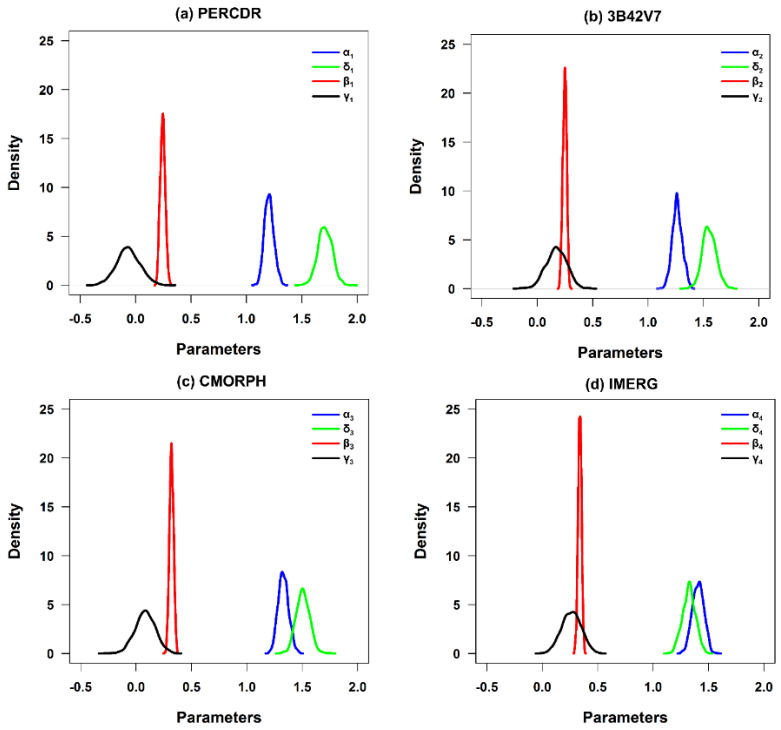

Figure 4: The PDF curves of posterior parameter sets with regard to (a) PERCDR, (b) 3B42V7, (c) CMORPH and (d) IMERG in the bias correction process of Stage 1.

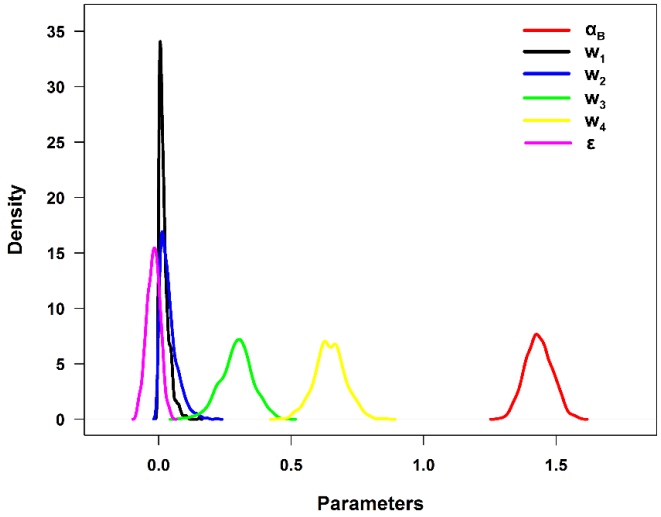

Figure 5: The PDF curves of posterior parameter sets in the data fusion process of Stage 2.

[2] In response to my comments, now in Section 2, it is mentioned that "The rain gauge data are spatially interpolated with a 0.25° x 0.25° resolution in the study region for each rainy day using

a bilinear interpolation approach. The 34 grid cells with the gauge sites are assumed as ground references (GR) in the blending process." This poses a serious limitation on the analysis. Given the complexity of the region, a simple bilinear interpolation approach is hard to justify. Look at figure 1, the elevation changes from 785 to 6252. The rain gauges stations are also far from each other, they are not dense.

Response: We thank the reviewer for this critical comment. We admit that the rain gauge stations are not very dense in the study area, but a denser ground network is not available in the short time. To address this significant concern, the China Gauge-based Daily Precipitation Analysis (CGDPA) at 0.25° and daily resolutions is replaced as the source of ground information in this study. The CGDPA is developed with a dense gauge network including 2400 rain gauges in mainland China using a climatology-based optimal interpolation and topographic correction algorithms (Shen and Xiong, 2014). The 34 grid cells with the gauge sites are assumed as ground references (GR) in the blending process. We have also rephrased the relevant statement in the revised manuscript (Lines 86-92).

Shen, Y. and Xiong, A.: Validation and comparison of a new gauge-based precipitation analysis over mainland China. Int. J. Climatol., 36, 252-265, 2016.

[3] In response to my comments, Authors wrote that "This study aims to develop a newly TSB algorithm on the multi-satellite precipitation data fusion in a certain time in regions of interest. Given that the larger challenge in the TP is to provide more accurate rainfall in a spatial domain, we are trying to overcome the shortage of limited rain gauge network based on the available SPE with spatial advantage using the TSB method in the NETP as a demonstration purpose. We agree that the satellite data are available for several years, but the exploration of long-term periods for the TSB method is another critical issue, e.g., the consideration of time impact on the fusion result." This response is hardly justified because Authors can repeat the validation for other years, especially when datasets are online available. Without this, I would have low confidence in most of the discussion in the result section.

Response: In the revision, the model performance is also validated with other years (2010-2013) as required by this reviewer. To address the reviewer's concern, model validation is performed under two scenarios: Scenario 1 will validate the model in space based on the data of the same period in validation stations (i.e., the 7 red grids in Figure 1), and Scenario 2 will validate the model in time based on the data of warm season from 2010 to 2013 at the same 27 black grids in

Figure 1. In addition, we consider a 10-fold cross validation in space by randomly selecting 7 sites for model validation, and the data of the remaining 27 sites as the training set. The performance of TSB approach is further compared with BMA and OOR in the two scenarios.

The model justification of the TSB approach are rephrased in the "*Section 4.2 Model validation under two scenarios"*, "*Section 4.3 Cross-validation"*, "*Section 4.4 Model comparison with BMA and OOR"*. Herein, Table 2 shows the summary of statistical error indices (i.e., RMSE, NMAE, and CC) of the original SPE (PERCDR, 3B42V7, CMORPH and IMERG), bias-corrected SPE (BC-PER, BC-V7, BC-CMO and BC-IME), and blended SPE under two scenarios. More details can be found in Lines 239-311 in the revised manuscript.

Table 2: Summary of statistical error indices (i.e., RMSE, NMAE, and CC) of the original, bias-corrected and blended SPE in two scenarios in the NETP.

Scenarios	Product	RMSE (mm/d)	NMAE (%)	CC
Scenario 1	PERCDR	7.15	70.2	0.382
	3B42V7	8.56	80.3	0.383
	CMORPH	6.25	60.6	0.556
	IMERG	6.60	62.9	0.506
	BC-PER	6.00	63.5	0.346
	BC-V7	5.83	61.4	0.408
	BC-CMO	5.43	56.3	0.533
	BC-IME	5.44	56.0	0.530
	Blended SPE	5.36	54.6	0.570
Scenario 2	PERCDR	9.19	79.3	0.261
	3B42V7	8.38	71.3	0.403
	CMORPH	7.20	61.9	0.493
	IMERG	7.64	65.1	0.462
	BC-PER	7.03	64.5	0.253
	BC-V7	6.69	61.3	0.395
	BC-CMO	6.41	58.2	0.480
	BC-IME	6.44	57.7	0.470
	Blended SPE	6.37	56.7	0.513

[4] Authors have tried to satisfy my comments by adding a small section on comparing the proposed approach with existing BMA and OOR approaches. There are no details on BMA and OOR. It is entirely left up to the readers to figure out all these from previous literature.

I am repeatedly asking for details because the research topic which Authors are trying to address in this manuscript is extremely challenging. If the selection of distribution, parameter estimation etc. have known drawbacks then demonstrating better values of RMSE, MAE and CC does not prove the efficacy of the TSB approach.

Response: We are thankful for this kind suggestion. The method details of BMA and ORR have been added in the "*Sections 3.2 Comparison Model"* in the revised manuscript as requested by this reviewer (Lines 186-209). In this study, the BMA approach makes use of four original satellite data and the corresponding GR data at the 27 black grids shown in Figure 1 in the warm season of 2014 to estimate the optimal BMA weights. In Scenario 1, the BMA data are calculated based on the BMA weights and the original SPE from the 7 red grids in the warm season of 2014, and the OOR data are calculated based on the OOR method using the original SPE data from the 7 red grids in the warm season of 2014. In Scenario 2, the BMA data are calculated based on the BMA weights and the original SPE from the 27 black grids in the warm season from 2010 to 2013, and the OOR result are calculated based on the OOR method and the original SPE data from the 27 black grids in the warm season from 2010 to 2013.

The description of BMA and OOR is repeated below:

*"**3.2 Comparison Model***

3.2.1 BMA

The BMA method is a statistical algorithm that merges predictive ensembles based on the individual SPE at the training period in regions of interest. Here, the BMA result refers to the ensemble SPE. Based on the law of total probability, the conditional probability of the BMA data on the individual SPE is expressed as:

$$f\left(BMA\middle|Y_1,\dots,Y_p\right)=\sum_{i=1}^{p}f(BMA|Y_i)\cdot w_i \qquad (17)$$

where $f(BMA|Y_i)$ is the predictive PDF given by the individual SPE Y_i and w_i is the corresponding weight. The log-likelihood function l is applied to calculate the BMA parameter set $\boldsymbol{\vartheta}$, which is written as:

$$l(\boldsymbol{\vartheta})=log\left(\sum_{i=1}^{p}w_i\times f(BMA|Y_i)\right) \qquad (18)$$

It is assumed that $f(BMA|Y_i)$ follows a Gaussian distribution with its parameters as θ_i, and BMA is ideally close to GR at any site and time. Eq. (18) is written as:

$$l(\boldsymbol{\vartheta}) = log(\sum_{i=1}^{p} w_i \times g(GR|\theta_i)) \quad (19)$$

where $g(\cdot)$ stands for Gaussian distribution, and $\boldsymbol{\vartheta} = \{w_i, \theta_i, i = 1, \dots, p\}$. The optimal BMA parameters $\boldsymbol{\vartheta}$ are calculated by maximizing the log likelihood function using the expectation–maximization algorithm. In this study, the training period is set as the warm season of 2014 in the NETP. Before the execution of the BMA method, both GR and SPE data are pre-processed using the Box-Cox transformation to ensure $f(BMA|Y_i)$ close to Gaussian distribution. As the BMA weights, $w_i, i = 1, \dots, 4$ are obtained, the BMA data is calculated by weighted sum of the original SPE at any site and time. More details of the BMA method can be learned from Ma et al. (2018).

3.2.2 OOR

The OOR method is defined as the arithmetic mean of the individual SPE by removing the feature with the largest offset. It is written as:

$$OOR = \frac{1}{p-1} \sum_{i=1}^{p-1} Y_i \quad (20)$$

where Y_i is the individual SPE, p is the number of SPE. In this experiment, the original SPE with the largest offset among the individuals is removed and the average of the remaining SPE is regarded as the OOR result in the regions of interest."

A two-stage blending approach for ~~blending~~ merging multiple satellite precipitation estimates and rain gauge observations: An experiment in the northeastern Tibetan Plateau

Yingzhao Ma[1], Xun Sun[2,3], Haonan Chen[1,4], Yang Hong[5], Yinsheng Zhang[6,7]

[1]Colorado State University, Fort Collins, CO 80523, USA
[2]Key Laboratory of Geographic Information Science (Ministry of Education), East China Normal University, Shanghai 200241, China
[3]Columbia Water Center, Earth Institute, Columbia University, New York, NY 10027, USA
[4]NOAA/Physical Sciences Laboratory, Boulder, CO 80305, USA
[5]School of Civil Engineering and Environmental Science, University of Oklahoma, Norman, OK 73019, USA
[6]Key Laboratory of Tibetan Environment Changes and Land Surface Processes, Institute of Tibetan Plateau Research, Chinese Academy of Sciences, Beijing, 100101, China
[7]CAS Center for Excellence in Tibetan Plateau Earth Sciences, Beijing, 100101, China

Correspondence to: Xun Sun (xs2226@columbia.edu)

Abstract. Substantial biases exist in the satellite precipitation estimates (SPE) over complex terrain regions and it has always been a challenge to quantify and correct such biases. The combination of multiple SPE and rain gauge observations would be beneficial to improve the gridded precipitation estimates. In this study, a two-stage blending (TSB) approach is proposed, which firstly reduces the systematic errors of ~~each~~ original SPE based on a Bayesian correction model, and then merges the bias-corrected SPE with a Bayesian ~~Bayesian~~ weighting model. In the first stage, the gauge-based observations are assumed as a generalized regression function of SPE and terrain feature. In the second stage, the relative~~SPE~~ weights of bias-corrected SPE are calculated based on the associated performances ~~relative to~~with ground references. The proposed TSB method has the ability to exert benefits from the bias-corrected SPE in terms of higher performance, and mitigate negative impacts from the ones with lower quality. In addition, Bayesian ~~analysis~~ analysis is applied in the two phases by specifying the prior distributions on model parameters, which enables to produce the posterior ensembles associated with their predictive uncertainties. The performance of the proposed TSB method is evaluated with independent validation ~~validation grids~~data in the warm season of 2010-2014 ~~4~~ in the northeastern Tibetan Plateau. Results show that the blended SPE is ~~significantly~~ greatly improved compared to the original SPE, ~~especially~~ even in the heavy rainfall event~~s~~. ~~.~~This study can ~~also~~ be expanded as a data fusion framework in the development of high-quality precipitation products in any regions of interest.

1 Introduction

High-quality precipitation data is fundamental to understand the regional and global hydrological processes. However, it is still difficult to acquire accurate precipitation information in the mountainous regions, e.g., Tibetan Plateau (TP), due to limited

ground sensors (Ma et al., 2015). The satellite sensors can provide precipitation estimates at a large scale (Hou et al., 2014), but performances of available satellite products vary among different retrieval methods and climate areas (Yong et al., 2015; Prat and Nelson, 2015; Ma et al., 2016). Thus, it is suggested to incorporate precipitation estimates from multiple sources into a fusion procedure with a full consideration of the strength of individual members and associated uncertainty.

Precipitation data fusion was initially reported by merging radar-gauge rainfall in the mid-1980s (Krajewski, 1987). The Global Precipitation Climatology Project (GPCP) was an earlier attempt for satellite-gauge data fusion, which adopted a mean bias correction method and an inverse-error-variance weighting approach to develop a monthly, 0.25° global precipitation data (Huffman et al., 1997). Another popular dataset, the Climate Prediction Center Merged Analysis of Precipitation (CMAP), included global monthly precipitation with a 2.5° x 2.5° spatial resolution for a 17-year period by merging gauges, satellites and reanalysis data using the maximum likelihood estimation method (Xie and Arkin, 1997). Since then, several blending approaches have been developed to generate gridded rainfall product with higher quality by merging gauge, radar and satellite observations (e.g., Li et al., 2015; Beck et al., 2017; Xie and Xiong, 2011; Yang et al., 2017; Baez-Villanueva et al., 2020). Overall, those fusion methods follow a general concept by eliminating biases in satellite/radar-based data and then merging the bias-corrected satellite/radar estimates with point-wise gauge observations. However, these efforts might be insufficient for quantifying the predicted data uncertainty. Some blended estimates are also partially polluted by the poorly performed individuals (Tang et al., 2018).

This paper develops a new ~~blending~~ data fusion ~~approach~~ method that enhances the quantitative modelling of individual error structures, prevents potential negative impacts from lower-quality members, and enables an explicit description of ~~the~~ model's predictive uncertainty. In addition, a Bayesian concept for accurate rainfall estimation is proposed based on these assumptions. The Bayesian analysis has the advantage of a statistically post-processing idea that could yield a predictive distribution with quantitative uncertainty (Renard, 2011; Shrestha et al., 2015). For ~~instance~~example, a Bayesian kriging approach, which assumes a Gaussian process of precipitation at any location and considers the elevation a covariate, is developed for merging monthly satellite and gauge precipitation data (Verdin et al., 2015). A dynamic Bayesian model averaging (BMA) method~~.~~, which shows better skill scores than the existing One-outlier removed (OOR) method, is applied for satellite precipitation data ~~merging~~ fusion across the TP (Ma et al., 2018; Shen et al., 2014). Given the ~~flexible distribution of~~ challenges of ~~multiple sources of~~ quantifying precipitation biases in regions with complex terrain (Derin et al., 2019), continuous efforts are required to exert the potential merit of Bayesian ~~approach~~ analysis on this critical issue.

In this ~~paper~~study, a two-stage blending (TSB) approach is ~~described~~ proposed for ~~combining~~ merging multiple satellite precipitation estimates (SPE) and ~~point-based rain gauge~~ground observations. The experiment is performed in the warm season (from May to September) ~~of~~ during 2010-2014 in the northeastern TP (NETP), where a relatively denser network of rain gauges is available compared to other regions of TP. The ~~proposed~~ TSB approach method is expected to help with the exploration of multi-source/scale precipitation data fusion in ~~other~~ regions with complex terrain.

The remainder of this paper is organized below: Section 2 describes the experiment including the study region and precipitation data ~~sets~~. Section 3 details the methodology, including the ~~proposed~~ TSB approach, and two existing fusion methods (i.e., BMA and OOR). Results and discussions are presented in Sections 4 and 5, respectively. The primary findings are summarized in Section 6.

2 Study area and data~~set~~

The study domain is located in the upper Yellow River basin of NETP (Fig. 1). As shown in the 90-m digital elevation data, the ~~elevation~~ altitude ranges from 785 m in the northeast to 6252 m in the southeast. The total annual precipitation is around 500 mm and the annual mean temperature is 0.7°C (Cuo et al., 2013). To avoid snowfall contamination on the gauge observation in the cold season, satellite and ground precipitation data from the warm season (May to September) of 2010 to 2014 are collected for the case study.~~To avoid snowfall contamination on the rain gauge observation in the cold season, the warm period from May 1 to September 30 in 2014 is selected for demonstration purpose.~~

Four mainstream SPE are used, including Precipitation Estimation from Remotely Sensed Information using Artificial Neural Networks - Climate Data Records (PERCDR) (Ashouri et al., 2015), Tropical Rainfall Measuring Mission (TRMM) Multi-satellite Precipitation Analysis (TMPA) 3B42 version 7 (3B42V7) (Huffman et al., 2007)~~.~~, National Oceanic and Atmospheric Administration (NOAA) Climate Prediction Centre (CPC) Morphing Technique Global Precipitation Analyses ~~Climate Prediction Center (CPC) Morphing technique for the bias-corrected research product version 1.0 (CMORPH)~~ Version 1 (CMORPH) (Xie et al., 2017~~Joyce et al., 2004~~), and the Integrated Multi-satellitE Retrievals for the Global Precipitation Measurement (GPM) mission ~~V03~~ V06 Level 3 final run product (IMERG) (Huffman et al., 2018). The basic information of SPE is shown in Table 1. ~~As th~~The IMERG has a 0.10° x 0.10° resolution, and other SPE have a spatial resolution of 0.25° x 0.25°. To eliminate the scale difference in the fusion process, the IMERG is resampled from 0.10° to 0.25° using the nearest neighbour interpolation method in advance.

The China Gauge-based Daily Precipitation Analysis (CGDPA) is used as the ground precipitation sources. It is developed based on a rain gauge network of 2400 gauge stations over Mainland China using a climatology-based optimal interpolation and topographic correction algorithms (Shen and Xiong, 2014). The 34 grid cells with the gauge sites in the regions of interest are assumed as ground references (GR), and~~A ground network including 34 rain gauges are used in this study. The gauge data are carefully checked to ensure its creditability (Shen and Xiong, 2016).~~ ~~A~~all ~~of of them~~ the grid cells are independent from the Global Precipitation Climatology Center (GPCC) stations, which are used for bias correction of the TRMM/GPM-era data (e.g., 3B42V7 and IMERG), and CMORPH (Huffman et al., 2007; Hou et al., 2014; ~~Joyce et al., 2004~~Xie et al., 2017).

~~The rain gauge data are spatially interpolated with a 0.25° x 0.25° resolution in the study region for each rainy day using a bilinear interpolation approach. The 34 grid cells with the gauge sites are assumed as ground references (GR) in the blending process. In addition, the GR are randomly classified into two parts: the black grids are used for training the model, and the red ones are used for model verification (Fig. 1). In order to clarify the TSB method, the selection of training cells is randomly repeated 10 times for the GR, and the remaining ones are used for model validation. Meanwhile, the TSB method is applied on a heavy rainfall event that occurred on September 22, 2014 to quantify its performance in extreme rainfall scenario. Local recycling plays as a premier role for the moisture sources of rainfall extremes in the NETP (Ma et al., 2020a). The September 22 rain case is a typical storm that can explain the local heavy rainfall patterns in the warm season. Meanwhile, the TSB method is applied on a heavy rainfall event that occurred on September 22, 2014 to quantify its performance in extreme rainfall scenario. The TSB approach is also compared with two existing fusion methods, i.e., BMA and One-outlier removed (OOR), which were previously applied for SPE data fusion in the TP (Ma et al., 2018; Shen et al., 2014).~~

3 Methodology

3.1 ~~The~~ TSB ~~algorithm~~

~~**3.1 Overview**~~

~~This algorithm aims at developing a multi-source data merging framework to provide the best-available gridded precipitation product with GR and SPE in the region of interest. Let $R(s,t)$ denote near-surface precipitation at the GR cell s and the t^{th} day. The original SPE and bias-corrected SPE are defined as $(Y_1(s,t), Y_2(s,t), \dots, Y_p(s,t)$ and $(Y_1^c(s,t), Y_2^c(s,t), \dots, Y_p^c(s,t))$ at the same grid and time. For simplicity, they are respectively replaced by R, $(Y_1, Y_2, \dots, Y_p)$, and $(Y_1^c, Y_2^c, \dots, Y_p^c)$. The subscript p implies the number of SPE, and PERCDR, 3B42V7, CMORPH and IMERG refer to Y_1, Y_2, Y_3, Y_4, respectively.~~

The diagram of the TSB method is shown in Figure 2. Stage 1 is designed to reduce the bias of the original SPE based on the GR at the training sites with a Bayesian correction (BC) procedure. In Stage 2, a Bayesian weighting (WS) model is used to merge the bias-corrected SPE.

3.1.1 Bias correction

(a) Model structure

~~Stage 1 is designed to mitigate the bias of the original SPE based on the GR at the training sites with a Bayesian correction (BC) procedure, where the assumption of probabilistic distribution for GR conditional on each SPE is not limited to Gaussian. Given complex terrain and 0.25° grid resolution, the topography is added as a covariate in the BC process. In the second stage, a Bayesian weight (BW) model is used to merge the bias-corrected SPE.~~ Let $R(s,t)$ denote near-surface precipitation at the GR cell s and the t^{th} day. The original SPE and bias-corrected SPE of PERCDR, 3B42V7, CMORPH and IMERG at the GR cell s and the t^{th} day are defined as $(Y_1(s,t), Y_2(s,t), \dots, Y_p(s,t)$ and $(Y_1'(s,t), Y_2'(s,t), \dots, Y_p'(s,t))$, respectively. For simplification purpose and without losing generality, these data at a particular GR cell and day will be denoted by R, (Y_1, Y_2, Y_3, Y_4), and (Y_1', Y_2', Y_3', Y_4'). While for all GR cells and days, they will be denoted in bold $\boldsymbol{R}$, $(\boldsymbol{Y_1}, \boldsymbol{Y_2}, \boldsymbol{Y_3}, \boldsymbol{Y_4})$, and $(\boldsymbol{Y_1'}, \boldsymbol{Y_2'}, \boldsymbol{Y_3'}, \boldsymbol{Y_4'})$. ~~The BW model can exert benefits from bias-corrected SPE with high performance and reduce poor impacts from the ones with lower quality. It also produces blended SPE with predictive uncertainty. The details of the TSB algorithm are described in Sections 3.2 and 3.3, respectively.~~

~~**3.2 Stage 1: Bias correction**~~

In ~~this~~ ~~s~~Stage 1, we perform ~~on~~ a conditional modelling of GR on each SPE, i.e., ~~on~~ the probabilistic distribution $f(R)$ ~~at the training sets~~ to improve the accuracy of the original SPE. Given that an appropriate assumption of $f(R)$ is necessary, ~~A flexible assumption (e.g., Lognormal, Gaussian, or Student's t distribution) for bias characteristics between GR and SPE is proposed. Given various SPE at different training sites, the specific probabilistic function is not limited to a certain distribution. T~~the goodness-of-fit of the Lognormal, Gaussian, and ~~Student's t~~Gamma distribution for the ~~bias between~~ GR ~~and SPE~~ is examined graphically by using a probability~~quantile-quantile~~probability (PP) plot at the training sets (Fig. 3). It is found that the usage of a Gamma distribution is more reliable as the associated PP plot is~~they are~~ closer to the diagonal ~~red~~ line than the others. For each satellite product, the Gamma distribution ~~A Student's t distribution is thus adopted with its mean parameter expressed as a linear regression of SPE. It~~ is parameterized as follows:

Formatted: Font: Bold
Formatted: Font: Bold
Formatted: Font: Italic
Formatted: Font: Bold, Italic

$$R \sim StudentGamma\left(\alpha_i, \frac{\alpha_i}{\mu_i}, \mu_i, \sigma_i\right) \quad (1)$$

where i is the number of satellite product. α_i, μ_i and $\frac{\alpha_i}{\mu_i}$ are the shape, mean and rate parameters of the Gamma distribution, respectively. Let the i^{th} SPE Y_i and the associated terrain feature Z be covariates related to the GR, the mean μ_i in Eq. (1) can be described with generalized linear regression of covariates Y_i and Z, which is written as follows:

$$\log(\mu_i) = \delta\alpha_i + \beta_i * \log(Y_i) + \gamma_i * Z \quad (2)$$

where Z, where ν_i is known as degree of freedom, μ_i and σ_i stand for sample mean and variance, respectively; the parameter μ_i is correlated with the intensity value of the i^{th} SPE (Y_i) and associated terrain feature (Z). To ignore the scale factor, the elevation feature in Eq. (2) is normalized and its value rangesing from 0 to 1, is the normalized elevation feature of each site after the normalization. $\boldsymbol{\theta_i\theta} = \{\nu_i, \alpha_i, \delta_i, \beta_i, \gamma_i, \sigma_i\}$ $(i = 1, \dots, 4)$ is summarized as a parameter set, which enables to write the likelihood function or probability density function (PDF) from Eqs. (1) and (2) conditional on $\boldsymbol{\theta}$ and Y_i as:

$$f(R|\boldsymbol{\theta}, Y_i) = \frac{\Gamma((\nu_i+1)/2)}{\Gamma(\nu_i/2)} \frac{1}{\sqrt{\nu_i\pi}\,\sigma_i}\left(1 + \frac{1}{\nu_i}\left(\frac{R-(\alpha_i+\beta_i*Y_i+\gamma_i*Z)}{\sigma_i}\right)^2\right)^{-(\nu_i+1)/2} \quad (3)$$

and will be estimated in Bayesian framework. In the following, $\boldsymbol{Z}$ will be denoted as the collection of the normalized elevation feature for all training data.

According to the Bayes's theorem, the posterior probability density function (PDF)distribution of parameter set $\boldsymbol{\theta_i\theta}$ given GR and SPE data, and the prior distribution of parameters $f(\boldsymbol{\theta})$ can be is expressed as:

$$f(\boldsymbol{\theta_i\theta}|\mathbf{R}, \boldsymbol{Y_i}, \boldsymbol{Z}) \propto f(\boldsymbol{R}|\boldsymbol{\theta_i\theta}, \boldsymbol{Y_i}, \boldsymbol{Z}) f(\boldsymbol{\theta_i\theta}) \quad (43)$$

where $f(\boldsymbol{\theta}_i)$ is the prior distribution and implies parameter information other than GR and SPE data, and $f(\boldsymbol{R}|\boldsymbol{\theta}_i, \boldsymbol{Y}_i, \boldsymbol{Z})$ is the likelihood function that defines the conditional probability of GR on the SPE and elevation. The priors of $f(\boldsymbol{\theta}_i)$ are initialized as Cauchy distribution with α_i in terms of its location at zero and scale as σ_{α_i} in Eq. (4), and Gaussian distribution with $\delta_i, \beta_i, \gamma_i$ in terms of its mean at zero and standard deviation (SD) at $\sigma_{\delta_i}, \sigma_{\beta_i}, \sigma_{\gamma_i}$ in Eqs. (5) - (7), respectively.

$$\alpha_i \sim Cauchy(0, \sigma_{\alpha_i}) \quad (4)$$

$$\delta_i \sim Normal(0, \sigma_{\delta_i}) \quad (5)$$

$$\beta_i \sim Normal(0, \sigma_{\beta_i}) \quad (6)$$

$$\gamma_i \sim Normal(0, \sigma_{\gamma_i}) \quad (7)$$

Formatted: Justified

Formatted: Font: Italic

Formatted: Justified

Formatted: Font: Not Bold

Formatted: Font: Not Bold

Given that the assumption of the weakly informative priors ensures the Bayesian inference in an appropriate range (Ma et al., 2020b), the hyper-priors of σ_{α_i}, σ_{δ_i}, σ_{β_i}, σ_{γ_i} are specified as 2, 10, 10, 10, respectively.

(b) Parameter estimation

The estimation of the posterior distribution $f(\boldsymbol{\theta}_i|\mathbf{R}, \boldsymbol{Y}_i, \boldsymbol{Z})$ in Eq. (3) becomes difficult challenging as its dimension grows with the number of parameters (Renard, 2011; Ma and Chandrasekar, 2020). Robertson et al. (2013) obtained the maximum a posteriori (MAP) solution for the model parameters using a stepwise method. Here, the Markov Chain Monte Carlo (MCMC) technique with is used to address this issue (Gelman et al., 2013)its sampling algorithm as the No-U-Turn Sampler (NUTS) variant of Hamiltonian Monte Carlo in the Stan program is performed to address this issue (Gelman et al., 2013). The sampling records of model parameters are obtained based on the training data in the warm season of 2014 in the NETP. Since we only have four parameters in this model, the MCMC converges very quickly. Thus, we run a chain of length 2000, removing the first 1000 iterations as the warm-up period and retaining the second 1000 iterations. The parameter samples of these 1000 iterations are the samples of the posterior distribution $f(\boldsymbol{\theta}_i|\mathbf{R}, \boldsymbol{Y}_i, \boldsymbol{Z})$. Figures 3a to 3dPDF in terms of PERCDR, 3B42V7, CMORPH and IMERR in this stage. Given that the assumption of the weakly informative priors ensures the Bayesian inference in an appropriate range (Ma et al., 2020b), the priors of $f(\boldsymbol{\theta})$ are initialized as uniform distribution with $\alpha_i, \beta_i, \gamma_i$ at real numbers in Eq. (5), and with ν_i, σ_i at a lower bound zero of real numbers in Eq. (6).

$$\alpha_i, \beta_i, \gamma_i \sim Uniform(-\infty, +\infty) \quad (5)$$

$$\nu_i, \sigma_i \sim Uniform(0, +\infty) \quad (6)$$

(c) Bayesian inference

Based on the estimated posterior distribution of parameter set $\boldsymbol{\theta}_i\boldsymbol{\theta}$ of each SPE, the next step is to calculateing the bias-corrected SPE R^* at any new site is of interest. It can be quantitatively simulated from its posterior distribution in Eq. (7) using the associatedoriginal SPE Y_i^*, normalized elevation Z_i^* and training data $\boldsymbol{R}, \boldsymbol{Y_i}, \boldsymbol{Z}$:

$$f(R^*|Y_i^*, Z_i^*, \boldsymbol{R}, \boldsymbol{Y}_i, \boldsymbol{Z}) = \int f(R^*, \boldsymbol{\theta}_i\boldsymbol{\theta}|Y_i^*, Z_i^*, \boldsymbol{R}, \boldsymbol{Y}_i, \boldsymbol{Z})\, d\boldsymbol{\theta}_i\boldsymbol{\theta} \quad (7)$$

Following the rule of joint probabilistic distributions, the right term inside the integral of Eq. (7) can beis written as:

$$f(R^*, \boldsymbol{\theta}_i\boldsymbol{\theta}|Y_i^*, Z_i^*, \boldsymbol{R}, \boldsymbol{Y}_i, \boldsymbol{Z}) = f(R^*|Y_i^*, Z_i^*, \boldsymbol{R}, \boldsymbol{Y}_i, \boldsymbol{Z}, \boldsymbol{\theta}_i\boldsymbol{\theta}) f(\boldsymbol{\theta}_i\boldsymbol{\theta}|Y_i^*, Z_i^*, \boldsymbol{R}, \boldsymbol{Y}_i, \boldsymbol{Z}Y_i^*, R, Y_i) \quad (8)$$

Formatted: Justified

Formatted: Font: Not Bold

Formatted: Font: Bold, Italic

Given that the new bias-corrected SPE R^* ~~Y_i^*~~ is independent ~~with R and Y_i~~ to the training data, the first term of the right side in Eq. (~~8~~9) is transformed as:

$$f(R^*|Y_i^*, Z_i^*, \boldsymbol{R}, \boldsymbol{Y}_i, \boldsymbol{Z}, \boldsymbol{\theta_i}\cancel{Y_i^*, R, Y_i,}\ \boldsymbol{\theta}) = f(R^*|Y_i^*, Z_i^*, \boldsymbol{\theta_i}\boldsymbol{\theta}) \quad (\cancel{9}10)$$

Since the parameters $\boldsymbol{\theta_i}\boldsymbol{\theta}$ are only dependent upon the training data $\boldsymbol{R}, \boldsymbol{Y_i}, \boldsymbol{Z}$, the second term of the right side in Eq. (~~8~~9) is expressed as:

Formatted: Font: Not Bold

$$f(\boldsymbol{\theta_i}|Y_i^*, Z_i^*, \boldsymbol{R}, \boldsymbol{Y}_i, \boldsymbol{Z})\cancel{(\boldsymbol{\theta}|Y_i^*, R, Y_i)} = f(\boldsymbol{\theta_i}\boldsymbol{\theta}|\boldsymbol{R}, \boldsymbol{Y_i}, \boldsymbol{Z}) \quad (\cancel{10}11)$$

Therefore, the ~~posterior~~ predictive ~~distribution~~ PDF of R^* in Eq. (~~7~~8) is written below:

$$f(R^*|Y_i^*, Z_i^*, \boldsymbol{R}, \boldsymbol{Y}_i, \boldsymbol{Z}\cancel{Y_i^*, R, Y_i}) = \int f(R^*|Y_i^*, Z_i^*, \boldsymbol{\theta_i}\cancel{Y_i^*, \boldsymbol{\theta}})f(\boldsymbol{\theta_i}|\boldsymbol{R}, \boldsymbol{Y}_i, \boldsymbol{Z})\cancel{(\boldsymbol{\theta}|R, Y_i)}\, d\boldsymbol{\theta_i}\boldsymbol{\theta} \quad (\cancel{11}12)$$

Since there is no general way to calculate the associated integral in Eq. (~~11~~12), the prediction~~it~~ is performed ~~again~~ using the MCMC ~~iterations~~iterated samplings (Renard, 2011). As for each SPE, ~~A~~a numerical algorithm is suggested below~~:~~, where n_{sim} ~~is assumed as~~stands for the replicate of the post-convergence MCMC samples and is set as 1000 in the case study~~.~~. Thus, ~~and t~~the predicted samples for R^* in Eq. (~~11~~12) are iterated (~~i~~ k = 1~~:, …, n_{sim}~~) n_{sim}) as follows:

1) For the i^{th} satellite product, randomly select a parameter sample~~Calculate the model parameters~~ $\boldsymbol{\theta_i}\boldsymbol{\theta} = \{\alpha_i, \delta_i, \beta_i, \gamma_i\}$ from the MCMC samples ~~Eqs. (1) to (6)~~;

~~2) Compute the mean parameter μ_i^* from the regression model of Eq. (2), i.e., $\log \mu_i^* = \alpha_i + \beta_i * Y_i^* + \gamma_i * Z^*$;~~

~~3~~2) Generate ~~the derived quantity~~a value R_k^*~~R^*~~ from ~~the posterior~~a ~~distribution~~ $Gamma\left(\alpha_i, \frac{\alpha_i}{\mu_i^*}\right)$~~of R^* in Eq. (11).~~, where $\log(\mu_i^*) = \delta_i + \beta_i * Y_i^* + \gamma_i * Z^*$;

Repeating step 1 and 2 for n_{sim} times, the samples R_k^* (k = 1:n_{sim}) are regarded as the realizations of the distribution of the bias-corrected SPE associated to the satellite estimation Y_i^* and normalized elevation Z^*. The mean value of the samples R_k^*, denoted by Y_i', is regarded as the bias-corrected SPE and the associated credible intervals (e.g., 2.5% and 97.5% quantiles) is used for predictive uncertainty.

3.1.~~3~~ 2 ~~Stage 2:~~ Data merging

Ideally, the blended SPE (B) should be close to GR, i.e., R. Given the Gamma distribution of GR in Step 1, the blended SPE can be parameterized below: ~~In Stage 1, the median value of the posterior samples is used as the bias-corrected SPE. Here, we redefine the bias-corrected SPE as $Y_i^{'}(i = 1,2,\dots,p)$. The formulas of blending the bias-corrected SPE are shown below:~~

$$B \sim Gamma\left(\alpha_B, \frac{\alpha_B}{\mu_B}\right) \quad (13)$$

where α_B, μ_B and $\frac{\alpha_B}{\mu_B}$ are the shape, mean and rate parameters, respectively. In this step, the bias-corrected SPE of 4 satellites are merged with weight parameters $w_i (i = 1, \dots, 4)$, and ε is the residual error. The data fusion of bias-corrected SPE specified in the log scale is defined as follows:

$$\log(\mu_B B) = \sum_{i=1}^{4} \log(Y_i') * w_i + \varepsilon \quad (14)$$

$$\sum_{i=1}^{4} w_i = 1 \quad (15)$$

~~$\sum_{i=1}^{p} w_i = 1$ (13)~~

$$\varepsilon \sim Normal(0, \sigma_\varepsilon) \quad (16)$$

~~$w_i \sim Uniform(0,1), i = 1, \dots, p$ (15)~~

~~$\sigma \sim Uniform(0, +\infty)$ (16)~~

~~where B is the blended SPE; w_i $(i=1,2,\dots,p)$ stands for the relative weight of the i^{th} bias-corrected SPE; ε is the residual error.~~ ~~Ideally, the blended SPE at the training site s and time t should be close to GR, i.e., $R(s, t)$.~~ Thereby, ~~model~~ all parameters ~~δ,~~ including $\alpha_B, w_i (i = 1,2,..p)$ and σ_ε ~~σ will~~ can be estimated ~~based on~~from the GR and bias-corrected SPE at the training sites. ~~With regard to the conditional distribution of blended SPE on the bias-corrected SPE, we propose a Gaussian distribution for the residual error modelling. The corresponding PDF is written as follows:~~

Formatted: Font: Italic
Formatted: Font: Italic
Formatted: Justified
Formatted: Font: Italic
Formatted: Justified
Formatted: Line spacing: Double

~~$f(B|\boldsymbol{\delta}) = \frac{1}{\sqrt{2\pi}\sigma}\exp\left(-\frac{1}{2}\left(\frac{B-\sum_{i=1}^{p} Y_i^t \cdot w_i}{\sigma}\right)^2\right)$ (17)~~

The estimation ~~calculation~~ process ~~of $\boldsymbol{\delta}$~~ in a Bayesian framework is similar to the~~at parameter estimation~~ described in ~~Stage 1~~the Stage 1. ~~, Figure 5PDF~~After all~~the~~ parameters ~~$\boldsymbol{\delta}$~~ are estimated, as similar to the Bayesian inference in Stage 1, ~~similar to Eqs. (7) to (11),~~ the blended SPE at any site and time ~~t~~ can be derived with the bias-corrected SPE and corresponding weights using the MCMC iterations.

~~Finally, we can obtain spatial patterns of blended SPE in terms of the median, standard deviation (SD) and associated credible intervals (e.g., 5% and 95% quantiles) in the regions of interest.~~

3.2 Comparison model

3.2.1 BMA

The BMA method is a statistical algorithm that merges predictive ensembles based on the individual SPE at the training period in regions of interest. Here, the BMA result refers to the ensemble SPE. Based on the law of total probability, the conditional probability of the BMA data on the individual SPE is expressed as:

$$f\left(BMA|Y_1,\dots,Y_p\right) = \sum_{i=1}^{p} f(BMA|Y_i)\cdot w_i \quad (17)$$

Formatted: Right

where $f(BMA|Y_i)$ is the predictive PDF given by the individual SPE Y_i and w_i is the corresponding weight. The log-likelihood function l is applied to calculate the BMA parameter set $\boldsymbol{\vartheta}$, which is written as:

Formatted: Font: Not Bold

$$l(\boldsymbol{\vartheta}) = \log\left(\sum_{i=1}^{p} w_i \times f(BMA|Y_i)\right) \quad (18)$$

It is assumed that $f(BMA|Y_i)$ follows a Gaussian distribution with its parameters as θ_i, and BMA is ideally close to GR at any site and time. Eq. (18) is written as:

~~log~~ ~~log~~ $l(\boldsymbol{\vartheta}) = \log(\sum_{i=1}^{p} w_i \times \mathrm{g}(GR|\theta_i))$ (19)

Formatted: Right

where $\mathrm{g}(\cdot)$ stands for Gaussian distribution, and $\boldsymbol{\vartheta} = \{w_i, \theta_i, i = 1,\dots,p\}$. The optimal BMA parameters $\boldsymbol{\vartheta}$ are calculated by maximizing the log likelihood function using the expectation–maximization algorithm. Before executing the BMA method, both GR and SPE data are pre-processed using the Box-Cox transformation to ensure that $f(BMA|Y_i)$ $(i = 1,\dots,4)$ is close to Gaussian distribution. As the BMA weights, $w_i, i = 1,\dots,4$ are obtained, the BMA data is calculated by weighted sum of the original SPE at any site and time. More details of the BMA method can be found in Ma et al. (2018).

3.2.2 OOR

The OOR method is defined as the arithmetic mean of the individual SPE by removing the feature with the largest offset. It is written as:

$$OOR = \frac{1}{p-1}\sum_{i=1}^{p-1} Y_i \quad (20)$$

where Y_i is the individual SPE, p is the number of SPE. The original SPE with the largest offset among the satellite products is removed and the average of the remaining SPE is regarded as the OOR result.

3.3 Error analysis

To assess the performance of the proposed TSB method, several statistical error indices including root mean square errors (RMSE), normalized mean absolute errors (NMAE), and the Pearson's correlation coefficients (CC) are used in this study. The specific formulas of these metrics can be found ~~in the literature (e.g., Chen et al., 2019 among others)~~below:

$$RMSE = \sqrt{<(Sim - Obs)^2>} \quad (21)$$

$$NMAE = \frac{<|Sim-Obs|>}{<Obs>} \times 100\% \quad (22)$$

$$CC = \frac{\sum[(Sim-<Sim>)(Obs-<Obs>)]}{\sqrt{\sum(Sim-<Sim>)^2}\sqrt{\sum(Obs-<Obs>)^2}} \quad (23)$$

where *Sim* and *Obs* stand for the simulated and observed data, respectively; the angle brackets stand for sample average.

4 Results

In the experiment, model parameters are calibrated on the daily precipitation of warm season in 2014, where GR data at the 27 black grids in Figure 1 are randomly selected for training the model. The model validation is performed under two scenarios: Scenario 1 will validate the model in space based on the data of the same period in validation stations (i.e., the 7 red grids in Figure 1), and Scenario 2 will validate the model in time based on the data of warm season from 2010 to 2013 at the same 27 black grids in Figure 1. In addition, we consider a 10-fold cross validation in space by randomly selecting 7 sites for model

Formatted: Font: 10 pt
Formatted: Font: 10 pt
Formatted: Right
Formatted: Font: 10 pt
Formatted: Font: 10 pt
Formatted: Font: 10 pt
Formatted: Font: 10 pt
Formatted: Font: 10 pt
Formatted: Font: 10 pt
Formatted: Font: 10 pt
Formatted: Font: 10 pt, Font color: Text 1
Formatted: Font: 10 pt, Font color: Text 1
Formatted: Font: 10 pt, Font color: Text 1
Formatted: Font: 10 pt, Font color: Text 1
Formatted: Font: 10 pt, Font color: Text 1
Formatted: Right

validation, and the data of the remaining 27 sites as the training set. The performance of TSB approach is further compared with BMA and OOR in the two scenarios.

4.1 Parameter estimates

Figures 4 and 5~~a to 4d~~ show~~s~~ the posterior distribution curves of the posterior parameters in Stage 1 and 2, respectively. As for each parameter in the bias-corrected process, the individual SPE including PERCDR, 3B42V7, CMORPH and IMERG shows similar ~~PDF~~ pattern (Figs. 4a to 4d). ~~in terms of PERCDR, 3B42V7, CMORPH and IMERR in this step, respectively. For each parameter, the individual SPE shows similar PDF curve.~~ It shows~~seems~~ that the bias structures of the original SPE have similar characteristics. For all SPE, the distribution mass of parameter β_i are all on the right side of zero, which implies that a systematic bias exists for all satellite products~~SPE~~. When looking at the effects of ~~In addition, the~~ elevation, the posterior distribution of parameter γ_i for PERCDR, 3B42V7 and CMORPH (Figs. 4a, 4b and 4c) have value zero in the middle range of the distribution, which implies that elevation may have little impacts on these three satellite products. While for~~ranges from 0.5~~ IMERG in Fig. 4d, the distribution mass of parameter γ_i is mostly on the right side of zero, which implies a clear effect of elevation on this satellite product. ~~to 0.5 among the satellite products, where the PDF pattern is similar between 3B42V7 and IMERG. It implies that the effect of elevation feature on the bias-corrected SPE has similar performance for 3B42V7 and IMERG.~~ In the data ~~merging~~fusion step (Fig. 5). IMERG has the highest weight and PERCDR has the lowest weight among the four bias-corrected SPE. Moreover, 3B42V7 and PERCDR have similar contribution on the blended result ~~(Fig. 5)~~. Basically, ~~the~~ Bayesian analysis is able to simulate the parameter uncertainty as ~~as~~ compared with the traditionally statistical method. ~~Figure 5 displays the PDF curves of the inferred posterior parameters in this step. It can be seen that the IMERG product has the highest weight and PERCDR has the lowest weight among the four bias-corrected SPE.~~

~~To assess the performance of the proposed TSB method, several statistical error indices including root mean square errors (RMSE), normalized mean absolute errors (NMAE), and the Pearson's correlation coefficients (CC) are used in this study. The specific formulas of these metrics can be found in the literature (e.g., Chen et al., 2019 among others).~~

4.~~1~~ 2 ~~Evaluation of the original, bias-corrected, and blended SPE~~Model validation under two scenarios

Table 2 presents the summary of the statistical error indices including RMSE, NMAE and CC of the original (i.e., PERCDR, 3B42V7, CMORPH and IMERG), bias-corrected (i.e., BC-PER, BC-V7, BC-CMO and BC-IME) and blended SPE under two

Formatted: Normal

Formatted: Heading 3

Formatted: Font: Not Bold

scenarios in the NETP. The sub-section 4.2.1 and 4.2.2 shows the performance of the model validation under Scenario 1 and 2, respectively.

Formatted: Font: Not Bold

4.2.1 Scenario 1

Formatted: Font: Bold

In Scenario 1, at the validation grids

Formatted: Normal

Compared to the GR, The original SPE show large biases at the validation grids in the NETP during the warm season of 2014 (Table 2). with Their statistical error metrics includingthe RMSE, NMAE, and CC indices rangeinge from 6.5925-8.0756 mm/d, 630.26-80.3.5%, and 0.4038 2-0.5568, respectively (Table 2). 3B42V7 has the worst skill with the highest RMSE of 8.0756 mm/d, and the highest NMAE of 80.3.5%, and the second lowest CC of 0.40383. CMORPHIMERG shows the best performance in terms ofwith the lowest RMSE of 6.25 mm/d, the lowest NMAE of 63.20.6% and the highest CC atof 0.5568, which presents its superiority compared with the other original SPE in the survey areaNETP.

Based on the BC model, all the bias-corrected SPE (i.e., BC-PER, BC-V7, BC-CMO and BC-IME) have better agreements with GR compared with the original SPE at the validation grids in the experiment. Their RMSE scores range from 4.5.463 to 5.06 mm/d, and decrease by 2713~371.38%, and their NMAE scores vary from 506.90 to 5863.75%, and decline by 197.11 to 231.15%, respectively, compared with the original SPE. Meanwhile, their CC values range from 0.34106 to 0.56833 after bias adjustmentcorrection (Table 2). Considering Given that the linear assumption of mean parameter in the Student's tGamma distribution at Stage 1in Stage 1 might fail to expect significant difference in the correlation, the CC value does not improve effectively for the bias-corrected SPE.

After Stage 2With the BW model, the blended SPE is closer to the GR in terms of RMSE, NMAE and CC at 45.346 mm/h, 4954.26%, and 0.60657, respectively, compared with both the original and bias-corrected SPE at the validation grid cells (Fig. 4). The RMSE and NMAE values of the blended SPE decrease by 3414.13~6537.4% and 2710.1~41.132%, respectively, and the CC value increases by 6.72.4~5049.42%, accordingly, compared towith the original SPE (Table 2). In addition,As eCompared with the bias-corrected SPE, the RMSE, NMAE and CC of the blended SPE increases by 51.14~140.28%, 32.35~164.21%, and 56.98~647.8%, in terms of RMSE, NMAE and CC, respectively, compared with the bias-corrected SPE. It is foundproves that the blended SPE exhibits higher quality at the validation grids after Stage 2, due to the ensemble contribution of the bias-corrected SPE with their relative weights at 0.0192, 0.05238, 0.2895, and 0.6407, respectively (Fig. 6a).. The BC-IME and BC-PER have the highest and lowest weights, respectively, and the contributions of BC-V7 and BC-CMO on the blended SPE rank between BC-IME and BC-PER (Fig. 5a). The relative weight of BC-PER, BC-V7, BC-CMO

and BC-IME is 0.02, 0.038, 0.295, and 0.647, respectively. The BC-IME and BC-PER have the highest and lowest weights, respectively, and the BC-V7 and BC-CMO rank between BC-IME and BC-PER (Fig. 6a). As for the original SPE, it is found that there is an overestimation when the rainfall is less than 7.6 mm/d, and an underestimation when the rainfall is more than 7.6 mm/d. Based on the proposed TSB approach, the blended SPE ~~has been~~is ~~effectively dropped~~closer towards the GR (Figs. 6b and 6c) ~~at the validation grids (Fig. 5b), especially for the rain intensity values less than 15 mm/d (Fig. 5c)~~. Meanwhile, BC-PER seems to be clearly different from the other bias-corrected SPE, and to this point in the study has shown little value to be kept in consideration in the merging process. However, it is worth noting that PERCDR can in fact be informative and on a case by case basis.

4.2.2 Scenario 2

~~Also, there is an overestimation in the original SPE but an underestimation in the blended SPE as the daily rainfall is more than 15 mm, partly because the BC process might over-correct the original SPE on the heavy rainfall. Overall, this TSB method has its ability to exert benefits from SPE in terms of higher performances and mitigate poor impacts from the ones with lower quality. Meanwhile, BC-PER seems to be clearly very different from the others, and to this point in the study has shown little value to be kept in consideration in the merging process. However, it is worth noting that PERCDR can in fact be informative and on a case by case basis.~~

The proposed TSB approach is also ~~examined~~validated in Scenario 2, where the blended SPE shows better performance in terms of its RMSE, NMAE and CC at 6.37 mm/h, 56.7% and 0.513, respectively, ~~as~~ compared with both the original and bias-corrected SPE. It shows that the original SPE including PERCDR, 3B42V7, CMORPH and IMERG have high RMSE and NMAE scores in terms of 7.20~9.19 mm/h and 61.9~79.3%, respectively, and low CC values in terms of 0.261~0.493. After the bias correction, the four satellite products have increased their performance with lower error indices than the original SPE. The RMSE indices of the bias-corrected SPE vary from 6.41 to 7.03 mm/h, and the corresponding NMAE and CC indices are from 57.7% to 64.5%, and from 0.253 to 0.48, respectively. Based on the data fusion process, the error indices of the blended SPE including RMSE, NMAE and CC are 6.37 mm/h, 56.7% and 0.513, respectively. It is found that the RMSE and NMAE values of the blended SPE decreased by 11.5~30.7% and 8.4~28.5%, respectively, and the CC value increases by 4.1~96.6% compared with the original SPE.

As learned from the two validated scenarios, it proves that

~~Overall,~~ the TSB approach has the potential in improving the satellite rainfall accuracy, and it has its ability to exert benefits from SPE in terms of higher performances and mitigate poor impacts from the ones with lower quality.

~~The results presented in Figures 6 are an average assessment of the TSB algorithm at all the validation grids, which can possibly homogenize some individual feature.~~

4.~~2~~3 Cross-validation ~~Model clarification with random validation grids~~

Figures 7 and 8 show the statistics of evaluation scores of RMSE, NMAE, and CC for the original SPE and blended estimates at the validation grids with 10 random split of the gauge locations in the warm season of 2014. For each test, 7 grid sites are randomly selected from the 34 grid cells and used for model verification, and the remaining 27 grid sites are used for training the model.

As for the blended SPE, it performs similar scores at the validation grids among the 10-fold random ~~tests~~samples~~,~~. ~~but~~The blended SPE shows better skill~~s~~ compared with the original SPE at each test in terms of RMSE, NMAE, and CC ~~at 4.34~5.57 mm/h, 49.2~61.7%, and 0.492~0.665, respectively, compared with the original SPE at each test~~ (Fig. 7). Statistically, the mean values of RMSE, NMAE and CC for the blended SPE are ~~4~~5.~~98~~75 mm/h, 5~~4~~7.~~9~~1% and 0.551~~97~~, respectively (Table 3). The averaged improvement ratios of RMSE for the blended SPE are ~~35~~27.~~1~~6%, ~~33~~25.~~7~~%, 1~~9~~0.6% and 13~~2.1~~% compared to the PERCDR, 3B42V7, CMORPH and IMERG, respectively, and similar performance is seen from NMAE with the average improvement ratios of 2~~94~~.~~85~~%, ~~30~~22.~~1~~3%, ~~1~~7.~~08~~% and ~~21~~7.3%, respectively (Table 4). In summary~~total~~, t~~T~~he 10-fold cross validation ~~random tests~~ further ~~clarify~~ verified that the blended SPE has a higher accuracy of gridded precipitation~~-~~ than the original satellite products~~which receives different credits from various SPE on an event basis~~.

4.4 Model comparison with BMA and OOR

To assess the performance of the proposed TSB approach, it is beneficial to compare the TSB result with the existing fusion approach. In this study, the BMA approach makes use of four original satellite data and the corresponding GR data at the 27 black grids shown in Figure 1 in the warm season of 2014 to estimate the optimal BMA weights. In Scenario 1, the BMA data are calculated based on the BMA weights and the original SPE from the 7 red grids in the warm season of 2014, and the OOR data are calculated based on the OOR method using the original SPE data from the 7 red grids in the warm season of 2014. In Scenario 2, the BMA data are calculated based on the BMA weights and the original SPE from the 27 black grids in the warm

season from 2010 to 2013, and the OOR result are calculated based on the OOR method and the original SPE data from the 27 black grids in the warm season from 2010 to 2013. Herein, we compare the blended SPE with both of the BMA and OOR predictions in two scenarios and their statistical error summary is shown in Table 5.

In Scenario 1, the TSB method performs better skill scores with the RMSE, NMAE and CC values of 5.36 mm/d, 54.6%, and 0.57, respectively, as compare with the BMA and OOR approaches. In addition, OOR shows the worst performance in terms of RMSE, NMAE, and CC at 6.22 mm/d, 59.7%, and 0.537, respectively. BMA shows better skill than OOR but worse skill than TSB, in terms of the RMSE, NMAE and CC values at 5.78 mm/d, 56.6% and 0.562, respectively. In Scenario 2, similar performance is found for the TSB approach, where it has lower RMSE (6.37 mm/d) and NMAE (56.7%) and higher CC (0.513) than both the OOR and BMA results. Basically, as compared with the two existing fusion algorithms (BMA and OOR) in the two validated scenarios, it confirms that the TSB method has an advantage for combining the original SPE and reducing the bias of the satellite precipitation retrievals.

~~**4.3 Model application in spatial domain**~~

Formatted: Font color: Text 1

~~It is important to explore the Bayesian ensembles at any unknown site in the study domain. Each SPE can capture the spatial pattern of daily mean precipitation in the warm season, but might fail in the representation of precipitation amount in the NETP (Fig. 9), partly because of the satellite retrieval bias in complex terrain and limited GR network. Here, the TSB approach is applied in spatial to obtain the blended SPE in terms of daily mean precipitation in the warm season of 2014 over the whole domain.~~

~~There is an overestimation for most of the original SPE, and the bias of the blended SPE is reduced based on the TSB approach. It is found that the blended SPE shows a better performance in terms of magnitude and distribution in the study area (Fig. 10a). Higher values disappear from the map except in southwest corner. The possible reason is that daily mean rainfall is the highest in southwest corner for each SPE, and higher value still exists after the TSB process. Meanwhile, the predictive uncertainties including SD, 5% and 95% quantiles are displayed from Figures 10b to 10d in order to illustrate the fusion variance.~~

4.4 5 Model performance on a Model performance during a hheavy rainfall case

Local recycling plays as a premier role for the moisture sources of rainfall extremes in the NETP (Ma et al., 2020a). The September 22, 2014 rain event is a storm that would represent the local heavy rainfall pattern in the warm season. Considering that Aaccurate precipitation on extreme weather is very important for flood hazard mitigation,. Wwe investigate the utility of this proposed TSB approach on this a heavy rainfall event case of September 22, 2014 over the NETP to quantify its performance in extreme rainfall case (Fig. 9a). . TThe relative weights of BC-PER, BC-V7, BC-CMO, and BC-IME for the blended data are 0.4264, 0.1243, 0.11291 and 0.340 15, respectively, on this particular heavy rainfall event (Fig. 9b). It is found that the IMERG data has the biggest contribution and the 3B42V7 and CMORPH data have nearly similar contribution for the blended SPE..

Table 56 reports the evaluation statistics reflecting the blended model performance during on this heavy rainfall case, where. It shows that tthe RMSE, NMAE and CC values of the original SPE range from 68.218~1094.4824 mm/d, 470.6~592.58%, and 0.68426~0.8205, respectively. As compared to the original SPE, the merged productblended SPE has lower RMSE of 45.123 mm/d, and lower NMAE of 2731.45%, and higherer CC of 0.850 37, respectively. In other words, tThe RMSE and NMAE values of the blended SPE decrease by 346.21~6043.64% and 32.53~5340.93%, respectively, and the CC index correspondingly increases by 3.4~23.9% on this heavy rainfall case compared to the original SPE.

The performance of the blended model performanceTSB approach is further explored at three gauge cells (i.e., IDs 56171, 56152 73, 56182067) with the top three daily rainfall records on September 22, 2014 (Fig. 10a). Figure 120 shows the PDF curves of blended samples at the above three grid sites in this rainfall case. It demonstrates the blended performance SPE onhas the advantage in quantifying the predictive uncertainty on rainfall extremes at each gridsite. For example, Aat ID 56171, the estimated rainfall derived from the original SPE are 19.8 mm (PERCDR), 35.3 mm (3B42V7), 26 mm (CMORPH), and 4021.2 mm (IMERG), respectively. 3B42V7 and IMERG shows an overestimation, while PERCDR and, CMORPH and IMERG underperform the daily rainfall at the corresponding pixel (Fig. 120a). Based on the TSB methodapproach, the median mean and SD value of the merging estimatesmerging estimates are 248.1 mm/d, and 4.4 mm/d, respectively. At IDs 56152 73 and 56182067, the median/SDmean values of the blended SPE are 24.3/5.026.2 mm/d and 19.721.9/4.5 mm/d, respectively, and they are very close to the GR with the daily amounts of 24.630.9 mm and 238.17 mm, respectively (Figs. 120b and 102c). Overall, Tthese analyses reveal that the proposed TSB method algorithm canould not only quantify its predictive uncertainty, but also improve the daily rainfall amount even underon rainfall extremes.

4.~~4 6~~6 Model application i~~n a Model performance during a h~~spatial domain

~~4.3 Model application in spatial domain~~

It is important to explore the Bayesian ensembles at ~~any~~ unknown site~~s~~ in the ~~study~~ domain. As learned from Figs. 11, it seems that ~~E~~each of the original SPE can capture the spatial pattern of daily mean precipitation in the warm season, but might fail in the representation of precipitation amount ~~in the NETP (Fig. 11~~), partly because of the satellite retrieval bias in complex terrain and limited GR network. Thus, the TSB method is further applied in the region of interest to demonstrate its performance on daily precipitation in the warm season of 2010-2014 in the NETP. ~~Here, the TSB approach is applied in spatial to obtain the blended SPE in terms of daily mean precipitation in the warm season of 2014 over the whole domain.~~

~~There is an overestimation for most of the original SPE, and the bias of the blended SPE is reduced based on the TSB approach.~~ It is found that ~~the~~the blended SPE shows high precipitation in the southwest and low precipitation in the northwest, as well as moderate precipitation in the eastern region. In addition, as compared with the original SPE, ~~a better performance in terms of magnitude and distribution in the study area (Fig. 12a). H~~higher values disappear from the spatial map except in southwest corner for the blended SPE. The possible reason is that daily mean rainfall is the highest in southwest corner for ~~each~~most SPE, and ~~higher~~larger value ~~still~~ exists after the TSB ~~process~~approach. Meanwhile, the predictive Bayesian uncertainties including lower (2.5%) and upper (97.5%) quantiles are displayed from Figures 1~~2~~2b to 1~~2~~2c ~~in order~~ to illustrate the ~~fusion~~blending variation~~ce~~ in this application.

~~4.5 Model comparison with other fusion methods~~

~~To assess the performance of the proposed TSB algorithm, it is beneficial to compare the TSB result with the existing fusion approach. Herein, we compare it with the BMA and OOR methods at the validation grids of NETP (red pixels in Figure 1) in the warm season of 2014 and their statistical error summary is shown in Table 6. It is found that the TSB method performs better skill with the RMSE, NMAE and CC values of 4.34 mm/d, 49.2%, and 0.606, respectively, compare with the other two fusion methods. OOR shows the worst performance in terms of RMSE, NMAE, and CC at 5.63 mm/d, 59.2%, and 0.547, respectively. As learned from model comparison among the three methods in this case, the TSB method has an advantage for combining the SPE and reducing the bias of the individuals.~~

5 Discussion

In spite of the superior performance of the TSB algorithm, some issues still need to be considered in the practical applications:

Because of limited knowledge on the influences of complex terrain and local climate on the rainfall patterns in the study area, the elevation feature is considered in the first stage. Table 7 quantifies the impact of elevation covariate on the bias-corrected and blended SPE performances ~~at the validation grids~~in Scenario 1 in the warm season of 2014 in the NETP. It is found that the inclusion of elevation feature provides slightly better skill compared with the results without terrain information in this experiment. Considering that deep convective systems occurring near the mountainous area have an effect on the precipitation cloud (Houze, 2012), more attempts are required to improve the orographic precipitation in the TP in future.

The data fusion application is based on four mainstream SPE, and ~~it is found that~~ BC-IME and BC-PER show the best and worst performances among the bias-corrected SPE in Stage 1. It raises a question that why not simply apply the first stage of bias correction and then select the best-performed bias-corrected SPE as the final product. To address this issue, we investigate the statistical error differences among the BC-IME and blended SPE before and after the removing of BC-PER for 10-fold cross validation ~~random verified tests~~ in the warm season of 2014 in the NETP (Figure 13). ~~It shows that i~~It is beneficial to involve the Stage 2 in the TSB method because the blended SPE performs better skill than the best-performed bias-corrected SPE (i.e., BC-IME) in ~~the Stage 1 process~~Stage 1. The primary reason is that the BW model is designed to integrate various types of bias-corrected SPE, which is limited in the BC model. ~~Also~~In addition, both the blended SPE with and without the consideration of PERCDR ~~in Figure 13~~ show similar performances of the RMSE, NMAE, and CC indices (Figure 13). It implies that the TSB approach has an advantage of not impacted by the poor quality individuals (e.g., BC-PER), partly because the BW model can reallocate the contribution of the bias-corrected SPE based on their corresponding bias characteristics.

In addition, as calculating the blended result at any new sites, the model parameters derived from the training grid sites are assumed to be applicable in the whole domain. Since we have a relatively dense GR network in the survey region, the current assumption is acceptable according to the performance of the blended SPE. It is helpful to give some guideline on how many training sites are needed to apply the TSB approach in a region with complex terrain and limited GR. The sensitivity analysis of the number of training grid cells on the performance of blended SPE at the validation grids is explored in Figure 14. As the number of training sites is increasing, there is a decreasing trend for the RMSE and NMAE values, but a slight increasing trend for the CC value. ~~Except for an anomaly with the No. 23, i~~It seems that the performance of the blended SPE becomes similar as the number of training sites increases to 21. We admit that the more information from the ground observations, it would be

more beneficial for the blended gridded product in the region of interest. It is noted that, if extended to the TP or global scale, the extension of model parameters and training sites should be carefully considered. For instance, there are few gauges installed in the western and central TP (Ma et al., 2015), it might be a potential risk to directly apply this fusion algorithm for these regions.

The aim of this study is not to model rainfall process in a target domain, but to propose an idea to extract valuable information from available SPE and provide more reliable gridded precipitation in high-cold region with complex terrain. Considering its spatiotemporal differences and the existence of many zero-value records, rainfall is extremely difficult to observe and predict (Yong et al., 2015; Bartsotas et al., 2018). With regard to the probability of rainfall occurrence, a zero-inflated model, which is coherent with the empirical distribution of rainfall amount, is expected to improve the proposed TSB algorithm. Also, hourly or even instantaneous precipitation intensity is extremely vital for flood prediction, which should be specifically designed when extending this fusion framework in the next step.

6 Summary and prospects

This study proposes a TSB algorithm for multi-SPE data fusion. A preliminary experiment is conducted in the NETP using four mainstream SPE (i.e., PERCDR, 3B42V7, CMORPH, and IMERG) to demonstrate the performance of this TSB approach. Primary conclusions are summarized below:

(1) This TSB algorithm has two stages and involves the BC and BW models. It is found that this blended method is capable of involving a group of original SPE ~~with their biases following different PDF curves~~. Meanwhile, it provides a convenient way to quantify the fusion performance and the associated uncertainty.

(2) The experiment shows that the blended SPE has better skill scores compared to the original SPE ~~at the validation locations~~in the two validated scenarios. The 10-fold cross validation ~~random tests~~ in Scenario 1 ~~also~~further confirms the superiority of the TSB algorithm. In addition, it is found that the TSB method outperforms another two existing fusion methods (i.e., BMA and OOR) in the two scenarios. The performance of this fusion method is ~~further~~ also demonstrated ~~using~~ under a heavy rainfall event in the region of interest. ~~In addition, the TSB method outperforms another two fusion methods (i.e., BMA and OOR).~~

(3) The application proves that this algorithm can allocate the contribution of individual SPE on the blended result because it is capable of ingesting useful information from uneven individuals and alleviating potential negative impacts from the poorly performing members.

Overall, this work provides an opportunity for merging SPE in high-cold region with complex terrain. The evaluation analysis of this TSB method for ~~long-term period and~~ extended regions (e.g., TP) in terms of higher temporal resolution (e.g., hourly) will be performed in a future study.

Data availability

The gauge data are from China Meteorological Data Service ~~Center~~Centre (http://data.cma.cn). The PERCDR data are obtained from http://www.ncei.noaa.gov/data/precipitation-persiann/; the CMORPH data are from https://rda.ucar.edu/datasets/ds502.2/; the 3B42V7 data are ~~obtained~~ from https://disc2.gesdisc.eosdis.nasa.gov/data/TRMM_L3/TRMM_3B42_Daily.7/~~https://pmm.nasa.gov/data-access/downloads/trmm~~; ~~the CMORPH data are obtained from ftp://ftp.cpc.ncep.noaa.gov/precip/CMORPH_V1.0;~~ the IMERG data are ~~obtained~~ from https://gpm1.gesdisc.eosdis.nasa.gov/data/GPM_L3/GPM_3IMERGDF.06/~~https://pmm.nasa.gov/data-access/downloads/gpm~~.

Author contributions

YM and XS conceived the idea; XS~~, YH,~~ and YZ acquired the project and financial supports. YM conducted the detailed analysis; HC, XS and YZ gave comments on the analysis; all the authors contributed to the writing and revisions.

Competing interests

The authors declare that they have no conflict of interest.

Acknowledgements

This study is supported by the National Key Research and Development Program of China (No. 2017YF~~A~~C~~0~~615~~0~~3~~1~~0~~0~~1) and~~,~~ Strategic Priority Research Program (A) of CAS (No. XDA2006020102)~~, and the National Natural Science Foundation of~~

~~China (No. 91437214). We also thank Dr. Ning Ma from the Institute of Tibetan Plateau Research, Chinese Academy of Sciences, for the great comments and suggestions.~~

References

Ashouri, H., Hsu, K. L., Sorooshian, S., Braithwaite, D. K., Knapp, K. R., Cecil, L. D., Nelson, B. R., and Prat O. P.: PERSIANN-CDR: Daily Precipitation Climate Data Record from Multisatellite Observations for Hydrological and Climate Studies, Bull. Amer. Meteor. Soc., 96, 69-83, 2015.

Baez-Villanueva, O. M., Zambrano-Bigiarini, M., Beck, H. E., McNamara, I., Ribbe, L., Nauditt, A., Birkel, C., Verbist, K., Giraldo-Osorio, J. D., and Thinh, N. X.: RF-MEP: A novel Random Forest method for merging gridded precipitation products and ground-based measurements, Remote Sens. Environ., 239, 111606, 2020.

Bartsotas, N. S., Anagnostou, E. N., Nikolopoulos, E. I., and Kallos, G.: Investigating satellite precipitation uncertainty over complex terrain, J. Geophys. Res.-Atmos., 123, 5346-5369, 2018.

Beck, H. E., van Dijk, A. I. J. M., Levizzani, V., Schellekens, J., Miralles, D. J., Martens, B., and de Roo A.: MSWEP: 3-hourly 0.25° global gridded precipitation (1979-2015) by merging gauge, satellite, and reanalysis data, Hydrol. Earth Syst. Sci., 21, 589-615, 2017.

~~Chen, H., Cifelli, R., Chandrasekar, V., and Ma, Y.: A flexible Bayesian approach to bias correction of radar-derived precipitation estimates over complex terrain: model design and initial verification, J. Hydrometeorol., 20, 2367-2382, 2019.~~

Cuo, L., Zhang, Y., Gao, Y., Hao, Z., and Cairang L.: The impacts of climate change and land cover/use transition on the hydrology in the upper Yellow River Basin, China, J. Hydro., 502, 37-52, 2013.

Derin, Y., Anagnostou, E., Berne, A., Borga, M., Boudevillain, B., Buytaert, W., Chang, C., Chen, H., Deirieu, G., Hsu, Y., Lavado-Casimiro, W., Manz, B., Moges, S., Nikolopoulos, E., Sahlu, D., Salerno, F., Rodriguez-Sanchez, J., Vergara, H., and Yilmaz, K.: Evaluation of GPM-era global satellite precipitation products over multiple complex terrain regions, Remote Sensing, 11, 2936, 2019.

Gelman, A., Carlin, J. B., Stern, H. S., Dunson, D. B., Vehtari, A., and Rubin D. B.: Bayesian Data Analysis-Third Edition, CPC Press. 2013.

Hou, A. Y., Kakar, R. K., Neeck, S., Azarbarzin, A. A., Kummerow, C. D., Kojima, M., Oki, R., Nakamura, K., and Iguchi, T.: The Global Precipitation Measurement Mission, Bull. Amer. Meteor. Soc., 95, 701-722, 2014.

Houze., R. A.: Orographic effects on precipitating clouds, Rev. Geophys., 50, RG1001, 2012.

Huffman, G., Adler, R., Arkin, P., Chang, A., Ferraro, R., Gruber, A., Janowiak, J. E., McNab, A., Rudolf, B., and Schneider, U.: The global precipitation climatology project (GPCP) combined precipitation dataset, Bull. Amer. Meteor. Soc., 78, 5-20, 1997.

Huffman, G. J., Bolvin, D. T., Nelkin, E. J., Wolff, D. B., Adler, R. F., Gu, G., Hong, Y., Bowman, K. P., and Stocker E. F.: The TRMM Multisatellite Precipitation Analysis (TMPA): quasi-global, multiyear, combined-sensor precipitation estimates at fine scales, J. Hydrometeorol., 8, 38-55, 2007.

Huffman, G. J., Bolvin, D. T., Braithwaite, D., Hsu, K., Joyce, R., Kidd, C., Nelkin, E. J., Sorooshian, S., Tan, J., and Xie, P.: NASA Global Precipitation Measurement (GPM) Integrated Multi-satellitE Retrievals for GPM (IMERG), Algorithm Theoretical Basis Document (ATBD) Version 5.2, NASA/GSFC, Greenbelt, MD, USA, 2018.

Joyce, R. J., Janowiak, J. E., Arkin, P. A. and Xie, P.: CMORPH: A method that produces global precipitation estimates from passive microwave and infrared data at high spatial and temporal resolution, J. Hydrometeorol., 5, 487-503, 2004.

Krajewski, W. F.: Cokriging radar-rainfall and rain gage data, J. Geophys. Res., 92, 9571-9580, 1987.

Li, H., Hong, Y., Xie, P., Gao, J., Niu, Z., Kirstetter, P. E., and Yong, B.: Variational merged of hourly gauge-satellite precipitation in China: preliminary results, J. Geophys. Res.-Atmos, 120, 9897-9915, 2015.

Ma, Y., Zhang, Y., Yang, D., and Farhan S. B.: Precipitation bias variability versus various gauges under different climatic conditions over the Third Pole Environment (TPE) region, Int. J. Climatol., 35, 1201-1211, 2015.

Ma, Y., Tang, G., Long, D., Yong, B., Zhong, L., Wan, W., and Hong, Y.: Similarity and error intercomparison of the GPM and its predecessor-TRMM Multi-satellite Precipitation Analysis using the best available hourly gauge network over the Tibetan Plateau, Remote Sensing, 8, 569, 2016.

Ma, Y., Hong, Y., Chen, Y., Yang, Y., Tang, G., Yao, Y., Long, D., Li, C., Han, Z., and Liu, R.: Performance of optimally merged multisatellite precipitation products using the dynamic Bayesian model averaging scheme over the Tibetan Plateau, J. Geophys. Res.-Atmos., 123, 814–834, 2018.

Ma, Y., Lu, M., Bracken, C., and Chen, H.: Spatially coherent clusters of summer precipitation extremes in the Tibetan Plateau: Where is the moisture from? Atmos. Res., 237, 104841, 2020a.

Ma, Y., Chandrasekar, V., and Biswas, S. K.: A Bayesian correction approach for improving dual-frequency precipitation radar rainfall rate estimates, J. Meteor. Soc. Japan, 98, 2020b.

Ma, Y., and Chandrasekar, V.: A Hierarchical Bayesian Approach for Bias Correction of NEXRAD Dual-Polarization Rainfall Estimates: Case Study on Hurricane Irma in Florida, IEEE Geosci. Remote. Sens. Lett, doi: 10.1109/LGRS.2020.2983041, 2020.

Prat, O. P., and Nelson, B. R.: Evaluation of precipitation estimates over CONUS derived from satellite, radar, and rain gauge data sets at daily to annual scales (2002–2012), Hydrol. Earth Syst. Sci., 19, 2037-2056, 2015.

Renard, B.: A Bayesian hierarchical approach to regional frequency analysis, Water Resour. Res., 47, W11513, 2011.

Robertson, D. E., Shrestha, D. L., and Wang, Q. J.: Post-processing rainfall forecasts from numerical weather prediction models for short-term streamflow forecasting. Hydrol. Earth Syst. Sci, 17, 3587-3603, 2013.

Sanso, B., and Guenni, L.: Venezuelan rainfall data analysed by using a Bayesian space time model, J. R. Stat. Soc. C.-Appl., 48, 345-362, 1999.

Shen, Y., and Xiong, A.: Validation and comparison of a new gauge-based precipitation analysis over mainland China, Int. J. Climatol., 36, 252-265, 2016.

Shen, Y., Xiong, A., Hong, Y., Yu, J., Pan, Y., Chen, Z., and Saharia, M.: Uncertainty analysis of five satellite-based precipitation products and evaluation of three optimally merged multi-algorithm products over the Tibetan Plateau. Int. J. Remote Sens., 35, 6843–6858, 2014.

Shrestha, D. L., Robertson, D. E., Bennett, J. C., and Wang, Q. J.: Improving Precipitation Forecasts by Generating Ensembles through Postprocessing. Mon. Weather Rev., 143, 3642-3663, 2015.

Tang, Y., Yang, X., Zhang, W., and Zhang, G.: Radar and Rain Gauge Merging-Based Precipitation Estimation via Geographical-Temporal Attention Continuous Conditional Random Field, IEEE Trans Geosci Remote Sens, 56, 1-14, 2018.

Tian, Y., Huffman, G. J., Adler, R. F., Tang, L., Sapiano, M., Maggioni, V., and Wu, H.: Modeling errors in daily precipitation measurements: additive or multiplicative, Geophy. Res. Lett., 40, 2060-2065, 2013.

Verdin, A., Rajagopalan, B., Kleiber, W., and Funk, C.: A Bayesian kriging approach for blending satellite and ground precipitation observations, Water Resour. Res., 51, 908-921, 2015.

Xie, P., and Arkin, P.: Global precipitation: a 17-year monthly analysis based on gauge observations, satellite estimates, and numerical model outputs, Bull. Amer. Meteor. Soc., 78, 2539-2558, 1997.

Xie, P., Xiong, A.-Y.: A conceptual model for constructing high-resolution gaugesatellite merged precipitation analyses, J. Geophys. Res.-Atmos. 116, D21106, 2011.

Formatted: English (United States)

Formatted: English (United States)

Xie, P., Joyce, S., Wu, S., Yoo, S., Yarosh, Y., Sun, F., and Lin, R.: Reprocessed, bias-corrected CMORPH global high-resolution precipitation estimates from 1998. J. Hydrometeor. 18, 1617-1641, 2017.

Yang, Z., Hsu, K., Sorooshian, S., Xu, X., Braithwaite, D., Zhang, Y., and Verbist, K.M.J.: Merging high-resolution satellite-based precipitation fields and point-scale rain gauge measurements - a case study in Chile, J. Geophys. Res.-Atmos., 122, 5267–5284, 2017.

Yong, B., Liu, D., Gourley, J. J., Tian, Y., Huffman, G. J., Ren, L., and Hong, Y.: Global View Of Real-Time Trmm Multisatellite Precipitation Analysis: Implications For Its Successor Global Precipitation Measurement Mission, Bull. Amer. Meteor. Soc., 96, 283-296, 2015.

Figure and Table Captions

Table 1: Basic information of the original SPE used in this study.

Table 2: Summary of statistical error indices (i.e., RMSE, NMAE, and CC) of the original, bias-corrected, and blended SPE in two scenarios in the NETP.

Table 3: Summary of the mean values of RMSE, NMAE and CC for the original and blended SPE at 10 random verified tests in the warm season of 2014 ~~over~~ in the NETP.

Table 4: Mean improvement ratios of statistical error indices of the blended SPE, in terms of RMSE, NMAE and CC compared with the original SPE at 10 random verified tests in the warm season of 2014 ~~over~~ in the NETP.

Table 5: Summary of statistical error indices (i.e., RMSE, NMAE, and CC) for three fusion methods (i.e., OOR, BMA, and TSB) in the two scenarios in the NETP.

Table ~~5~~6: Summary of statistical error indices (i.e., RMSE, NMAE, and CC) for the original and blended SPE during a heavy rainfall event of ~~over the NETP on~~ September 22, 2014 in the NETP.

~~**Table 6:** Summary of statistical error indices (i.e., RMSE, NMAE, and CC) in terms of three fusion methods (i.e., OOR, BMA, and TSB) at the validated grid cells of NETP in the warm season of 2014.~~

Table 7 Summary of statistical error indices (i.e., RMSE, NMAE, and CC) for bias-corrected and blended SPE with and without consideration of terrain feature as a covariate in the TSB method in Scenario 1 in the NETP~~at the validation grids of NETP in the warm season of 2014~~.

Figure 1: Spatial map of the topography and GR network used in the study, where 27 black cells are used for model calibration and 7 red cells are for model verification.

Figure 2: The diagram of the proposed TSB algorithm.

Figure 3: (a) The histogram density plot and (b) the corresponding Probability-Probability plot of GR at the training grids in the warm season of 2014 in the NETP, where the red, blue and green lines shows the fitted Gamma, Lognormal and Gaussian distribution, respectively.

Figure 4: The PDF curves of posterior parameter sets with regard to (a) PERCDR, (b) 3B42V7, (c) CMORPH and (d) IMERG in the bias correction process, i.e., Stage 1.

~~Quantile-quantile plots at training sets for the bias between GR and SPE, where (a) to (d) shows PERCDR, 3B42V7, CMORPH, and IMERG, respectively.~~ **Figure 5**: The PDF curves of posterior parameter sets in the data fusion process, i.e., Stage 2.

Formatted: English (United States)

~~**Figure 4:** Intercomparisons of statistical error indices for the original, bias-corrected, and blended SPE at the validation grids in the warm season of 2014: (a) RMSE, (b) NMAE, and (c) CC.~~

Figure ~~5~~6: (a) The Box-Whisker plots of relative weights for the bias-corrected SPE, (b) the scatter plots between GR and the original SPE and (c) the PDF of daily rainfall for the GR, original and blended SPE with various rain intensities in Scenario 1 in the NETP.~~(a) The Box-Whisker plots of relative weights of the bias-corrected SPE in Stage 2; (b) Scatter plots between GR and various SPE (original and blended) at the validation grids in the warm season of 2014; (c) The PDF of daily rainfall in terms of the GR, original and blended SPE with various intensities at the validation grids in the warm season of 2014.~~

~~**Figure 6:** Time series of daily rainfall estimates and rainfall accumulations at a selected validation grid with the maximum rainfall record in the warm season of 2014: (a) daily rainfall estimates, and (b) rainfall accumulations.~~

Figure 7: Statistical error indices of the original and blended SPE at 10 random verified tests ~~for 10 random tests~~ in the warm season of 2014 in the NETP: (a) RMSE, (b) NMAE~~,~~ and (c) CC.

Figure 8: The Box-Whisker plots of improvement ratios of statistics for the blended SPE compared with the original SPE, including PERCDR, 3B42V7, CMORPH, and IMERG at 10 random verified tests ~~for 10 random tests~~ in the warm season of 2014 in the NETP: (a) RMSE, (b) NMAE~~,~~ and (c) CC.

~~**Figure 9:** Spatial patterns of the daily mean precipitation in terms of the original SPE in the warm season of 2014: (a) PERCDR, (b) 3B42V7, (c) CMORPH, and (d) IMERG.~~

~~**Figure 10:** Spatial patterns of the blended SPE in terms of (a) median, (b) SD, (c) 5% and (d) 95% quantiles of daily mean precipitation in the warm season of 2014.~~

Figure ~~11~~9: (a) Spatial pattern of gauge-based measurements during a heavy rainfall case ~~over the NETP on~~of September 22, 2014 in the NETP, where the site IDs 56171, 56173 and 56067 report the top three daily rainfall amounts of 32.3 mm, 30.9 mm and 28.7 mm~~56152 and 56182 report the top three daily rainfall amounts of 30.4 mm, 24.6 mm and 23.1 mm~~, respectively; (b) the corresponding Box-Whisker plots of relative weights of the ~~individual~~ bias-corrected SPE in the ~~Stage 2~~data fusion process.

Figure 12: The PDF curves of blended SPE samples and the corresponding median value at three gauge-based sitgrides duringon a heavy rainfall case onof September 22, 2014: (a) ID 56171, (b) ID 561527273, and (c) ID 561822067. The original SPE and GR at each pixel are also indicated in each subfigure.

Figure 11: Spatial patterns of the daily mean precipitation in terms of the original SPE in the warm season of 2010 to 2014 in the NETP: (a) PERCDR, (b) 3B42V7, (c) CMORPH, and (d) IMERG.

Figure 12: Spatial patterns of the blended SPE in terms of (a) mean, (b) lower quantile (2.5%) and (c) upper quantile (97.5%) of daily mean precipitation in the warm season of 2010 to 2014 in the NETP.

Figure 13. Statistical error indices (i.e., RMSE, NMAE, and CC) of the best-performed bias-corrected SPE (i.e., BC-IME, black) and blended SPE before (red) and after (blue) removing the worst-performed BC-PER at 10 random verified tests for 10 random verified tests in the warm season of 2014 in the NETP.

Figure 14: Statistical error indices (i.e., RMSE, NMAE, and CC) of the blended SPE at the validation grid locations in terms of different number of training sites in the warm season of 2014 in the NETP.

Table 1: Basic information of the original SPE used in this study.

Short name	Full name and details	Temporal resolution	Spatial resolution	Input data	Retrieval algorithm	References
PERCDR	Precipitation Estimation from Remotely Sensed Information using Artificial Neural Networks (PERSIANN) Climate Data Record (CDR)	Daily	0.25° x 0.25°	Warm season from 2014.50 to 2014.9	Adaptive artificial neural network	*Ashouri et al.*, 2015
3B42V7	TRMM Multi-satellite Precipitation Analysis (TMPA) 3B42 Version 7	3 hourlyDaily	0.25° x 0.25°	Warm season from 2010 to 2014 2014.5-2014.9	GPCC monthly gauge observation to correct this bias of 3B42RT	*Huffman et al.*, 2007
CMORPH	NOAA Climate Prediction Centre (CPC) Climate Prediction Center (CPC) MorphORPHing tTechnique (CMORPH) for bias-corrected product version 1.0Global Precipitation Estimates Version 1	3 hourlyDaily	0.25° x 0.25°	Warm season from 2010 to 2014 2014.5-2014.9	Morphing technique	*XieJoyce et al.*, 20041704
IMERG	Integrated Multi-satellitE Retrievals for the Global Precipitation Measurement (GPM) mission V036 Level 3 final run product	0.5 hourlyDaily	0.10° x 0.10°	Warm season from 20102014.5 to 2014.9	20147 version of the Goddard profiling algorithm	*Huffman et al., 2018*

Table 2: Summary of statistical error indices (i.e., RMSE, NMAE, and CC) of the original, bias-corrected~~, bias-corrected,~~ and blended SPE ~~at the validation grids of NETP in the warm season of 2014~~in two scenarios in the NETP.

Scenarios	Product	RMSE (mm/d)	NMAE (%)	CC
Scenario 1	PERCDR	7.~~36~~15	7~~4~~0.~~6~~2	0.~~416~~382
	3B42V7	8.~~07~~56	8~~3~~0.~~5~~3	0.~~40~~383
	CMORPH	6.~~59~~25	6~~7~~0.~~5~~6	0.~~493~~556
	IMERG	~~7~~6.~~18~~60	6~~3~~2.~~2~~9	0.5~~60~~86
	BC-PER	6.00	63.5	0.346
	BC-V7	5.83	61.4	0.408
	BC-CMO	5.43	56.3	0.533
	BC-IME	5.44	56.0	0.530
	~~BC-PER~~	~~**5.02**~~	~~**58.7**~~	~~**0.418**~~
	~~BC-V7~~	~~**5.06**~~	~~**57.5**~~	~~**0.410**~~
	~~BC-CMO~~	~~**4.81**~~	~~**54.6**~~	~~**0.497**~~
	~~BC-IME~~	~~**4.56**~~	~~**50.9**~~	~~**0.572**~~
	Blended SPE	~~4~~5.~~34~~36	~~49~~54.~~2~~6	0.~~606~~570
Scenario 2	PERCDR	9.19	79.3	0.261
	3B42V7	8.38	71.3	0.403
	CMORPH	7.20	61.9	0.493
	IMERG	7.64	65.1	0.462
	BC-PER	7.03	64.5	0.253
	BC-V7	6.69	61.3	0.395
	BC-CMO	6.41	58.2	0.480

BC-IME	6.44	57.7	0.470
Blended SPE	6.37	56.7	0.513

730

Formatted: Font: Not Bold, English (United Kingdom)
Formatted: Font: 10 pt, Not Bold, English (United Kingdo
Formatted: English (United Kingdom)
Formatted: Font: 10 pt, English (United Kingdom)
Formatted: English (United Kingdom)
Formatted: Font: 10 pt, English (United Kingdom)
Formatted: English (United Kingdom)
Formatted: Font: 10 pt, English (United Kingdom)
Formatted: Font: 10 pt, English (United Kingdom)
Formatted: Centered
Formatted: Font: Not Bold, English (United Kingdom)
Formatted: Font: 10 pt, Not Bold, English (United Kingdo
Formatted: English (United Kingdom)
Formatted: Font: 10 pt, English (United Kingdom)
Formatted: English (United Kingdom)
Formatted: Font: 10 pt, English (United Kingdom)
Formatted: English (United Kingdom)
Formatted: Font: 10 pt, English (United Kingdom)

Table 3: Summary of the mean values of RMSE, NMAE and CC for the original and blended SPE at 10 random verified tests in the warm season of 2014 in the NETP.

Product	RMSE (mm/d)	NMAE (%)	CC
PERCDR	7.~~72~~96	7~~8~~.5.9	0.3~~78~~30
3B42V7	7.~~57~~72	73.8.~~9~~	0.~~433~~424
CMORPH	6.~~21~~59	6~~6~~.3.1	0.5~~13~~20
IMERG	~~76~~.3~~7~~8	~~70~~62.7.~~0~~	0.5~~72~~18
Blended SPE	~~4~~5.~~98~~75	5~~4~~7.~~9~~1	0.5~~97~~51

735

Table 4: Mean improvement ratios of statistical error indices of the blended SPE, in terms of RMSE, NMAE, and CC compared with the original SPE at 10 random verified tests in the warm season of 2014 ~~over~~ in the NETP.

	Index	PERCDR	3B42V7	CMORPH	IMERG
Improvement Ratio (%)	RMSE (mm/d)	~~35~~27.~~1~~6	~~33~~25.~~7~~0	1~~9~~0.6	1~~3~~2.~~1~~0
	NMAE (%)	2~~9~~4.~~8~~5	~~30~~22.~~1~~3	~~1~~7.~~0~~8	~~2~~17.3
	CC	~~61~~71.~~3~~1	3~~9~~.8.~~2~~	1~~7~~1.~~5~~1	~~4~~10.~~3~~7

Table 5: Summary of statistical error indices (i.e., RMSE, NMAE, and CC) for the original and blended SPE during a heavy rainfall event over the NETP on September 22, 2014.

Product	RMSE (mm/d)	NMAE (%)	CC
PERCDR	6.28	40.6	0.822
3B42V7	10.12	59.5	0.686
CMORPH	6.80	45.6	0.734
IMERG	10.48	53.3	0.805
Blended SPE	4.13	27.4	0.850

Table ~~6~~5: Summary of statistical error indices (i.e., RMSE, NMAE, and CC) for three fusion methods (i.e., OOR, BMA, and TSB) ~~at the validation grids of NETP in the warm season of 2014~~in the two scenarios in the NETP.

Scenarios	Method	RMSE (mm/d)	NMAE (%)	CC
Scenario 1	OOR	56.6322	59.27	0.54737
	BMA	5.4478	576.66	0.59562
	TSB	45.346	4954.26	0.606570
Scenario 2	OOR	7.04	59.9	0.498
	BMA	6.79	58.8	0.500
	TSB	6.37	56.7	0.513

745

Formatted: Font: 10 pt, English (United Kingdom)
Formatted Table
Formatted: English (United Kingdom)
Formatted: English (United Kingdom)
Formatted: English (United Kingdom)
Formatted: Font: Bold, English (United Kingdom)
Formatted: Font: Bold, English (United Kingdom)
Formatted: Font: Bold, English (United Kingdom)
Formatted: Font: Not Bold, English (United Kingdom)
Formatted: English (United Kingdom)
Formatted: English (United Kingdom)
Formatted: Font: Not Bold, English (United Kingdom)
Formatted: English (United Kingdom)
Formatted: Font: Not Bold, English (United Kingdom)
Formatted: English (United Kingdom)
Formatted: English (United Kingdom)
Formatted: Font: 10 pt, Not Bold, English (United Kingdo
Formatted: English (United Kingdom)
Formatted: English (United Kingdom)
Formatted: Font: Not Bold, English (United Kingdom)
Formatted: English (United Kingdom)
Formatted: Font: 10 pt, Not Bold, English (United Kingdo
Formatted: English (United Kingdom)
Formatted: English (United Kingdom)
Formatted: Font: 10 pt, Not Bold, English (United Kingdo
Formatted: English (United Kingdom)

Table 6: Summary of statistical error indices (i.e., RMSE, NMAE, and CC) for the original and blended SPE during a heavy rainfall event of September 22, 2014 in the NETP.

Product	RMSE (mm/d)	NMAE (%)	CC
PERCDR	8.18	47.0	0.850
3B42V7	9.24	52.8	0.683
CMORPH	8.27	48.5	0.734
IMERG	8.63	49.1	0.642
Blended SPE	5.23	31.5	0.837

Table 7 Summary of statistical error indices (i.e., RMSE, NMAE, and CC) for bias-corrected and blended SPE with and without consideration of terrain feature as a covariate in the TSB method ~~at the validation grids of NETP~~in Scenario 1 ~~in the warm season of 2014~~in the NETP.

Product	Type	RMSE (mm/d)	NMAE (%)	CC
BC-PER	No Terrain	~~55~~.~~03~~98	~~58~~63.3~~.9~~	0.~~416~~361
	Terrain	~~56~~.~~02~~00	~~58~~63.~~7~~5	0.3~~418~~6
BC-V7	No Terrain	5.~~0~~83	~~58~~61.~~0~~5	0.40~~3~~9
	Terrain	5.~~06~~83	~~57~~61.~~5~~4	0.4~~1~~08
BC-CMO	No Terrain	~~45~~.~~83~~48	5~~5~~6.~~0~~9	0.~~493~~520
	Terrain	~~45~~.~~81~~43	5~~4~~.6.3	0.~~497~~533
BC-IME	No Terrain	~~4~~.5.~~4~~8	5~~1~~6.~~4~~3	0.5~~68~~19
	Terrain	~~45~~.~~56~~44	5~~0~~6.~~9~~0	0.5~~72~~30
Blended SPE	No Terrain	~~45~~.~~36~~41	~~49~~55.~~7~~0	0.~~603~~557
	Terrain	~~45~~.~~34~~36	5~~4~~9.~~2~~6	0.~~606~~570

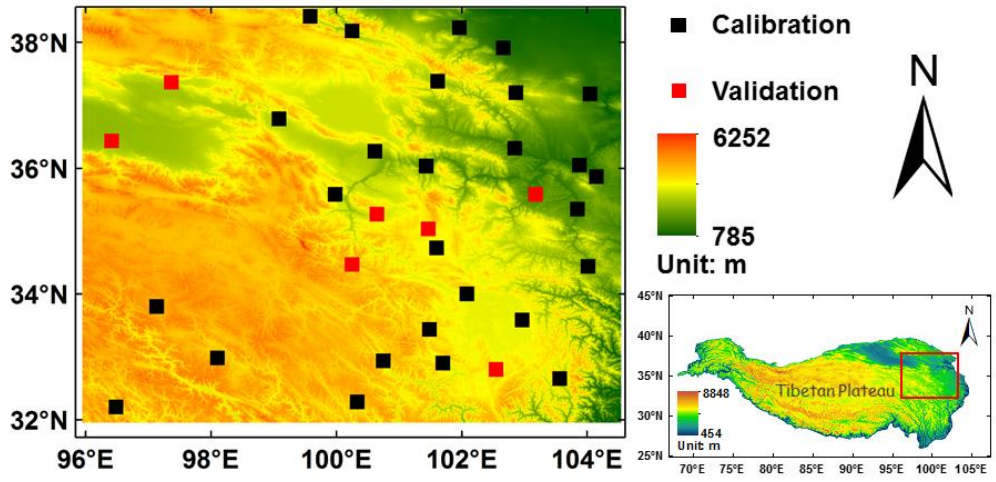

Figure 1: Spatial map of the topography and GR network used in the study, where 27 black cells are used for model calibration and 7 red cells are for model verification.

760

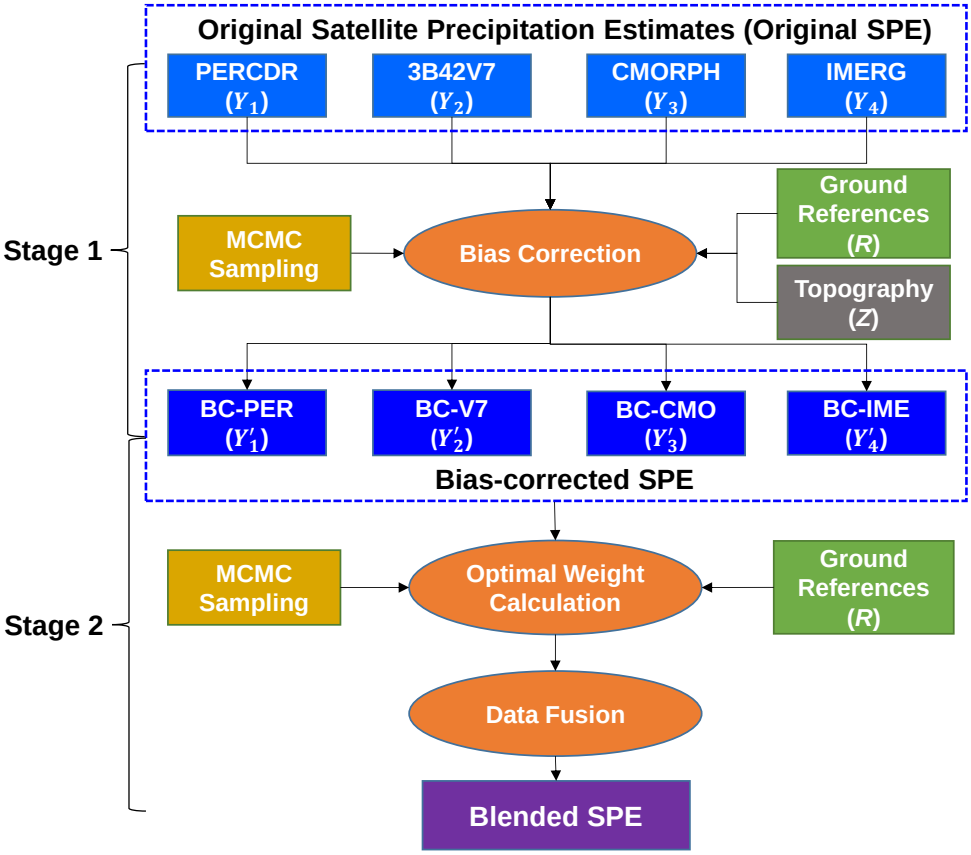

Figure 2: The diagram of the proposed TSB algorithm.

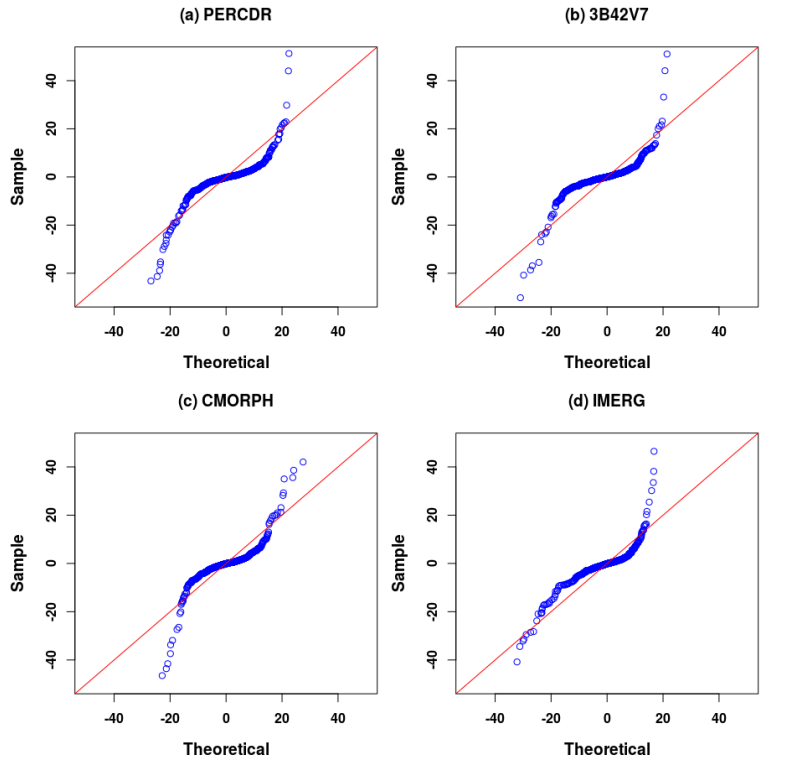
(a) PERCDR
(b) 3B42V7
(c) CMORPH
(d) IMERG
Sample
Theoretical
-40
-20
0
20
40

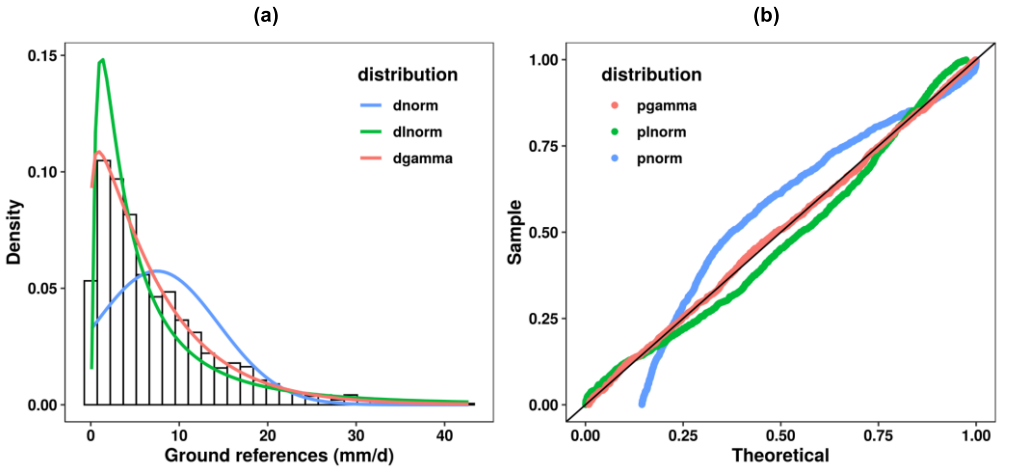

765

Figure 3: (a) The histogram density plot and (b) the corresponding Probability-Probability plot of GR at the training grids in the warm season of 2014 in the NETP, ~~Quantile-quantile plots at the training sets for the bias between GR and SPE,~~ where ~~(a) to (d)~~the red, blue and green lines shows ~~PERCDR, 3B42V7, CMORPH, and IMERG~~the fitted Gamma, Lognormal and Gaussian distribution, respectively.

Formatted: Justified, Line spacing: Double

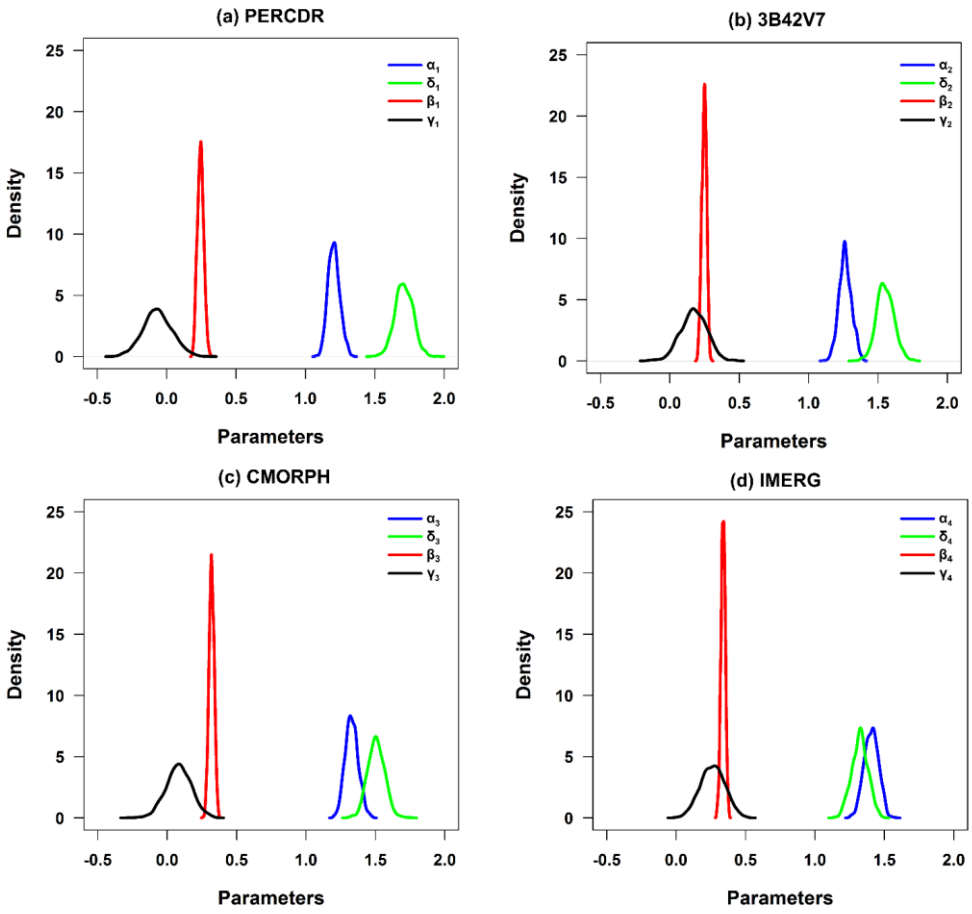

Figure 4: The PDF curves of posterior parameter sets with regard to (a) PERCDR, (b) 3B42V7, (c) CMORPH and (d) IMERG in the bias correction process of Stage 1.

Formatted: Font: Bold

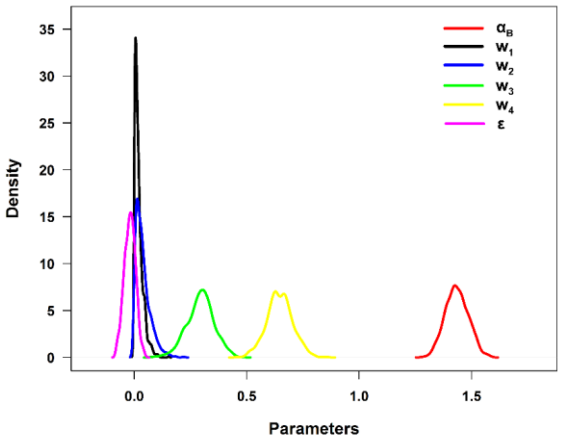

Figure 5: The PDF curves of posterior parameter sets in the data fusion process of Stage 2.

775

Formatted: Centered

Formatted: Font: Bold

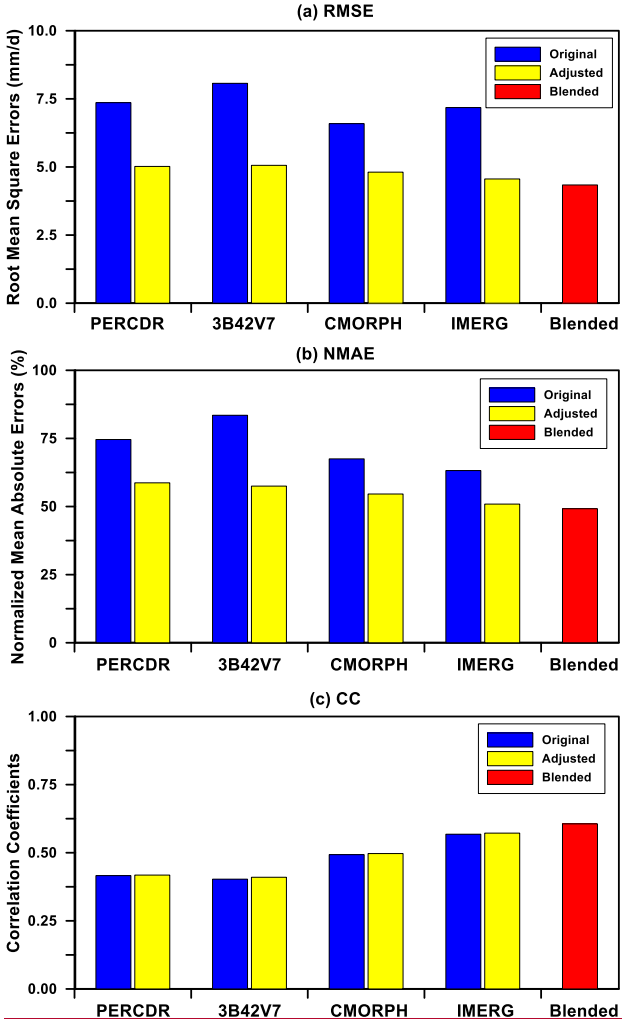

~~**Figure 4:** Intercomparison of statistical error indices for the original, bias-corrected, and blended SPE at the validation grids in the warm season of 2014: (a) RMSE, (b) NMAE, and (c) CC.~~

Formatted: Centered, Line spacing: single

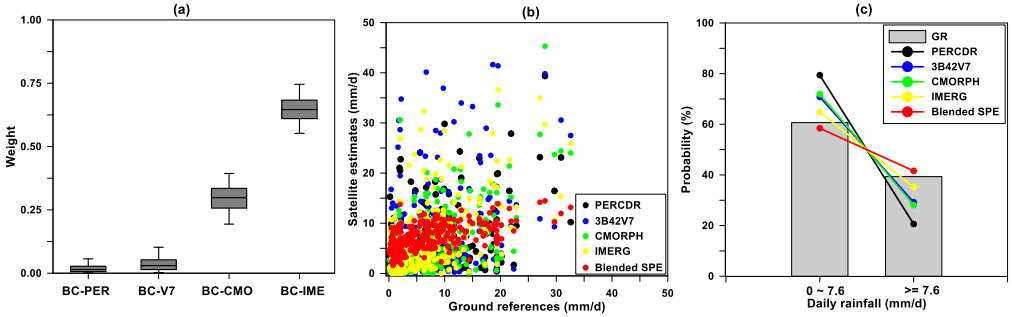

780

Figure 6: (a) The Box-Whisker plots of relative weights for the bias-corrected SPE, (b) the scatter plots between GR and the original SPE and (c) the PDF of daily rainfall for the GR, original and blended SPE with various rain intensities in Scenario 1 in the NETP.

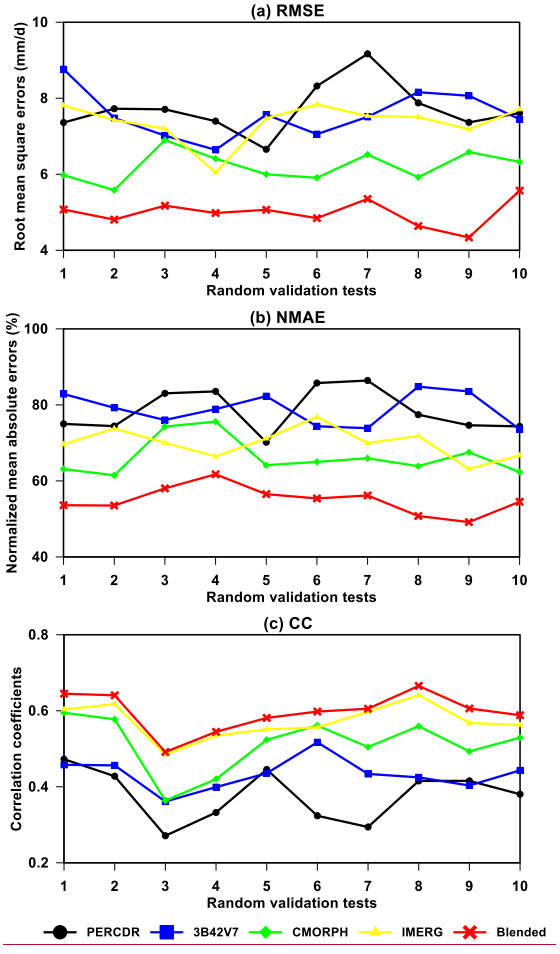

Formatted: Line spacing: single

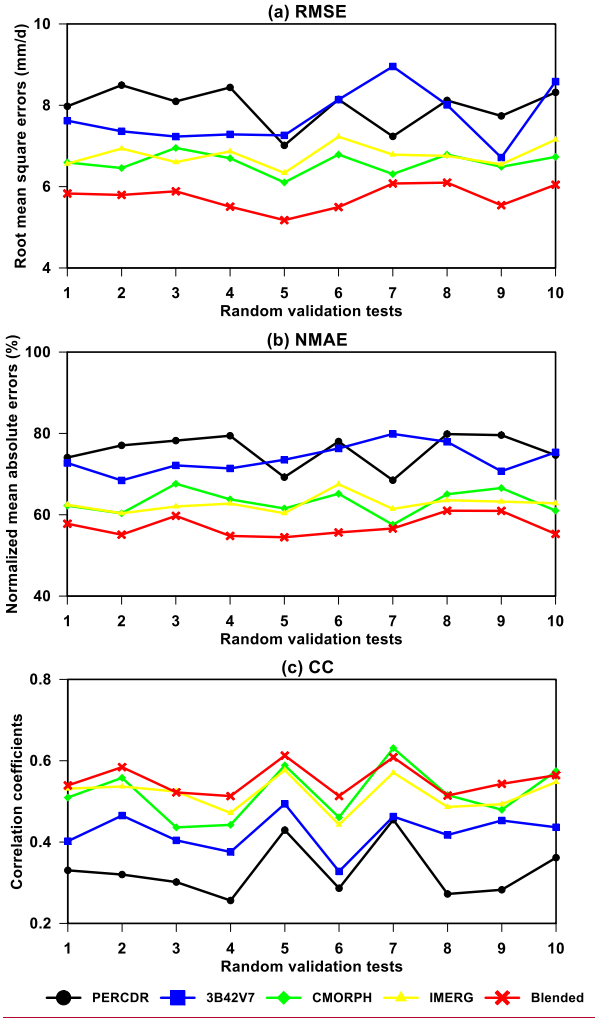

Figure 7: Statistical error indices of the original and blended SPE at 10 random verified tests ~~for 10 random tests~~ in the warm season of 2014 in the NETP: (a) RMSE, (b) NMAE~~,~~ and (c) CC.

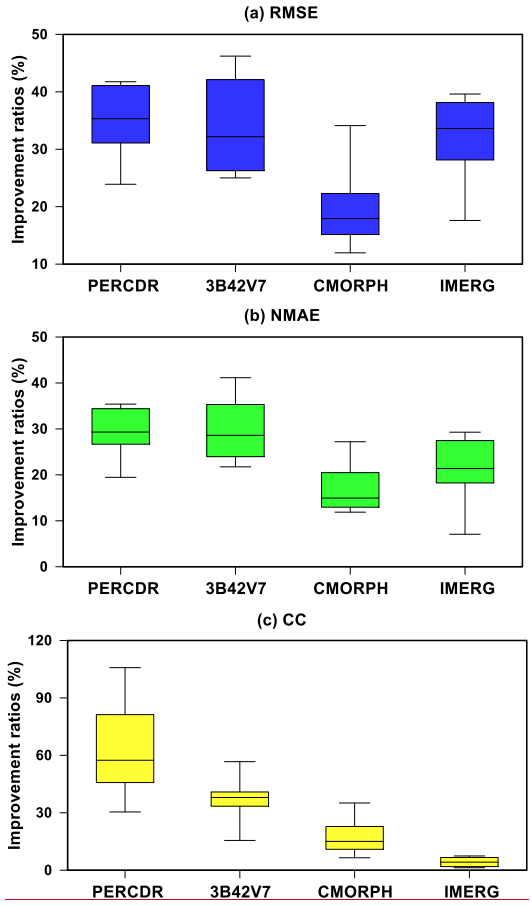
(a) RMSE
Improvement ratios (%)
50
40
30
20
10
PERCDR
3B42V7
CMORPH
IMERG
(b) NMAE
Improvement ratios (%)
50
40
30
20
10
0
PERCDR
3B42V7
CMORPH
IMERG
(c) CC
Improvement ratios (%)
120
90
60
30
0
PERCDR
3B42V7
CMORPH
IMERG

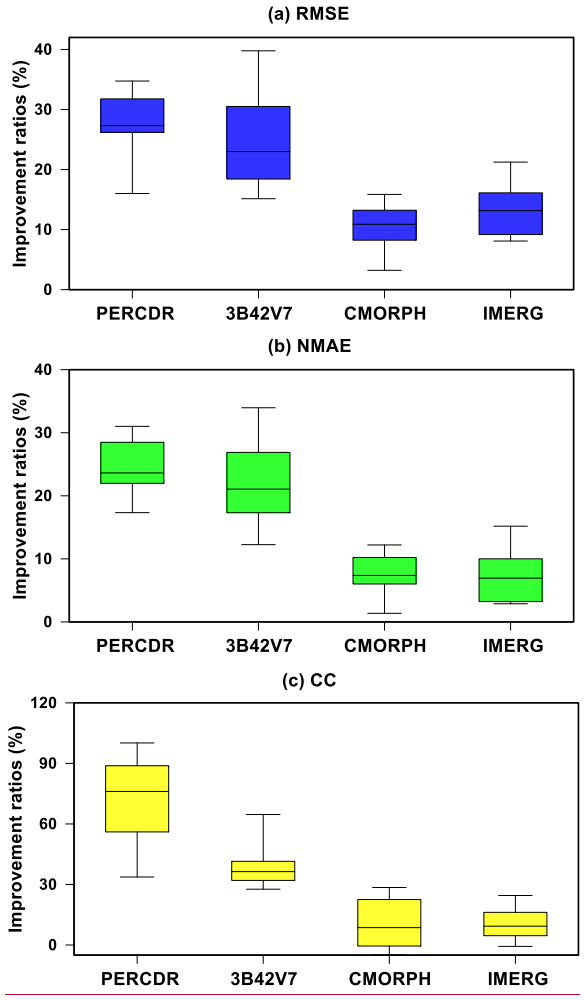

Figure 8: The Box-Whisker plots of improvement ratios of statistics for the blended SPE compared with the original SPE, including PERCDR, 3B42V7, CMORPH, and IMERG ~~for 10 random tests~~ at 10 random verified tests in the warm season of 2014 in the NETP: (a) RMSE, (b) NMAE~~,~~ and (c) CC.

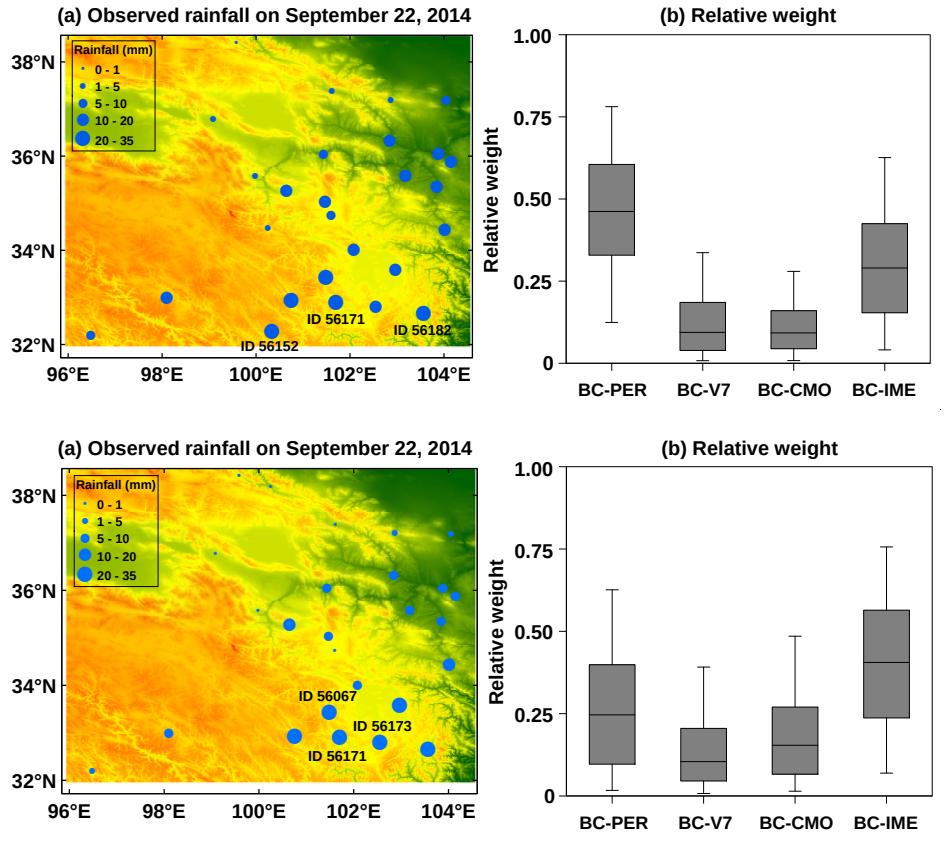

Figure ~~11~~9: (a) Spatial pattern of gauge-based measurements during a heavy rainfall case ~~over the NETP on~~ of September 22, 2014 in the NETP, where the site IDs 56171, 561~~5~~723 and 561~~82~~067 report the top three daily rainfall amounts of 3~~0~~2.~~4~~3 mm, 2~~4~~30.~~6~~9 mm and 2~~3~~8.~~1~~7 mm, respectively; (b) the corresponding Box-Whisker plots of relative weights ~~of~~of the ~~individual~~ bias-corrected SPE in the ~~Stage 2~~data fusion process.

Formatted: Left, Line spacing: single

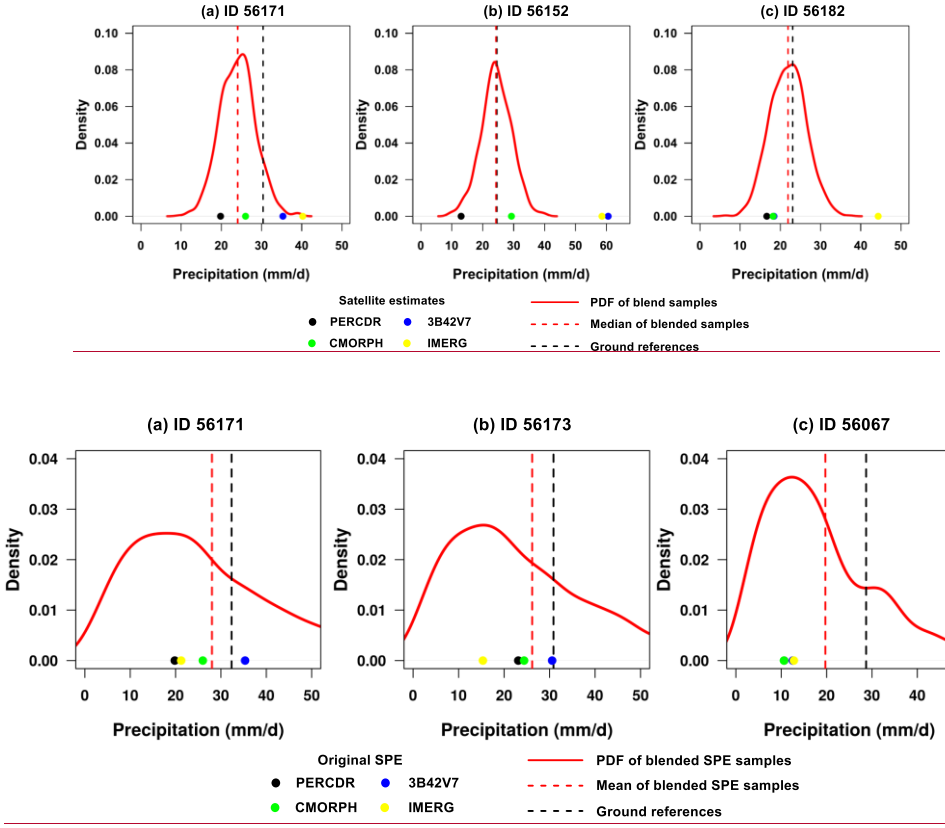

Figure 1~~2~~0: The PDF curves of blended SPE samples and the corresponding ~~median~~ mean value at three gauge-based ~~sites~~ grids ~~during~~ on a heavy rainfall case ~~on~~ of September 22, 2014: (a) ID 56171, (b) ID ~~56152~~56173~~,~~ and (c) ID ~~56182~~56067. The original SPE and GR at each pixel are also indicated in each subfigure.

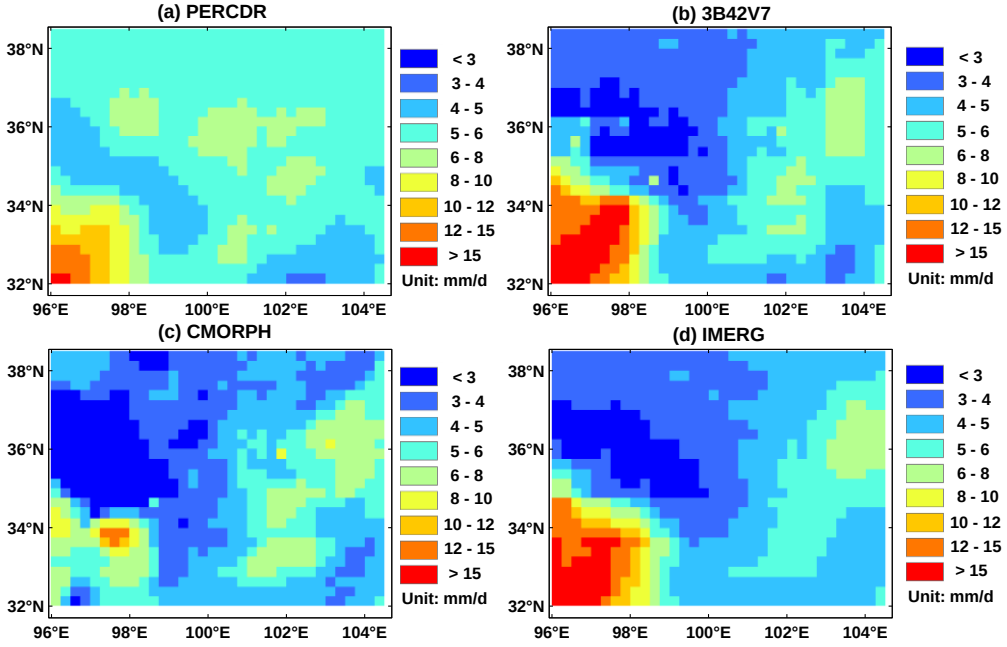

Figure 11: Spatial patterns of the daily mean precipitation in terms of the original SPE in the warm season of 2010 to 2014 in the NETP: (a) PERCDR, (b) 3B42V7, (c) CMORPH, and (d) IMERG.

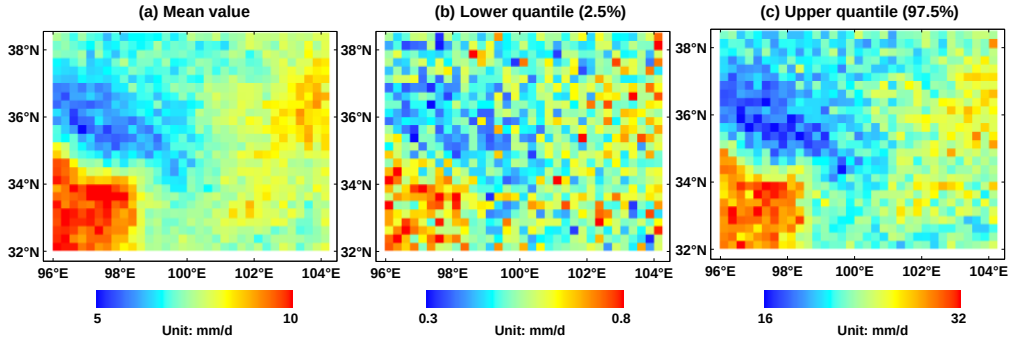

Figure 12: Spatial patterns of the blended SPE in terms of (a) mean, (b) lower quantile (2.5%) and (c) u~~U~~pper quantile (97.5%) of daily mean precipitation in the warm season of 2010 to 2014 in the NETP.

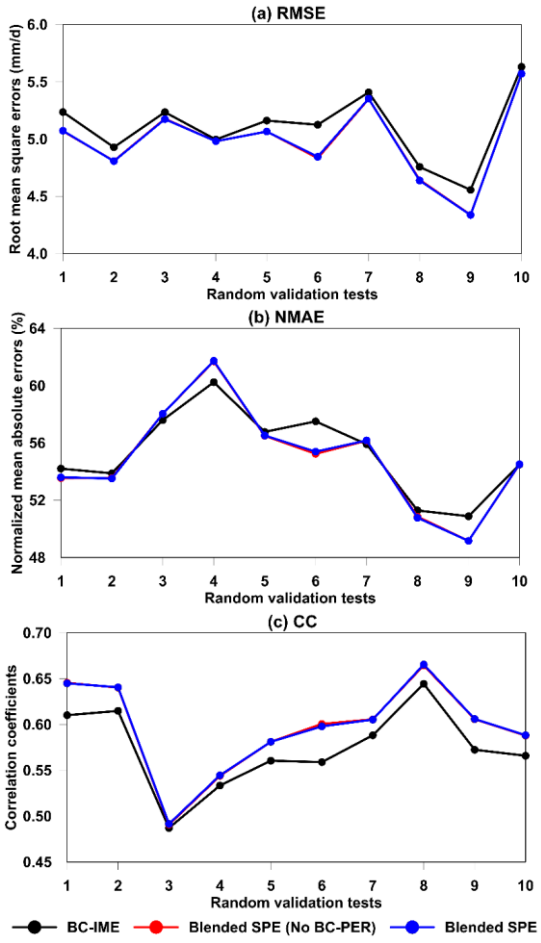
(a) RMSE
Root mean square errors (mm/d)
6.0
5.5
5.0
4.5
4.0
1 2 3 4 5 6 7 8 9 10
Random validation tests
(b) NMAE
Normalized mean absolute errors (%)
64
60
56
52
48
1 2 3 4 5 6 7 8 9 10
Random validation tests
(c) CC
Correlation coefficients
0.70
0.65
0.60
0.55
0.50
0.45
1 2 3 4 5 6 7 8 9 10
Random validation tests
BC-IME
Blended SPE (No BC-PER)
Blended SPE

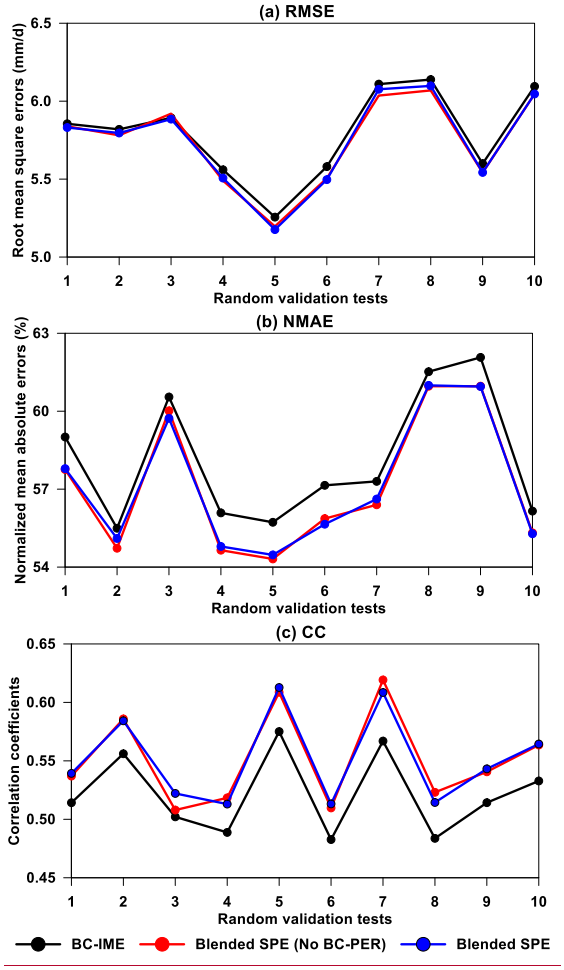

Figure ~~13~~13: Statistical error indices (i.e., RMSE, NMAE, and CC) of the best-performed bias-corrected SPE (i.e., BC-IME, black) and blended SPE before (red) and after (blue) removing the worst-performed BC-PER at 10 random verified tests ~~for 10 random verified tests~~ in the warm season of 2014 in the NETP.

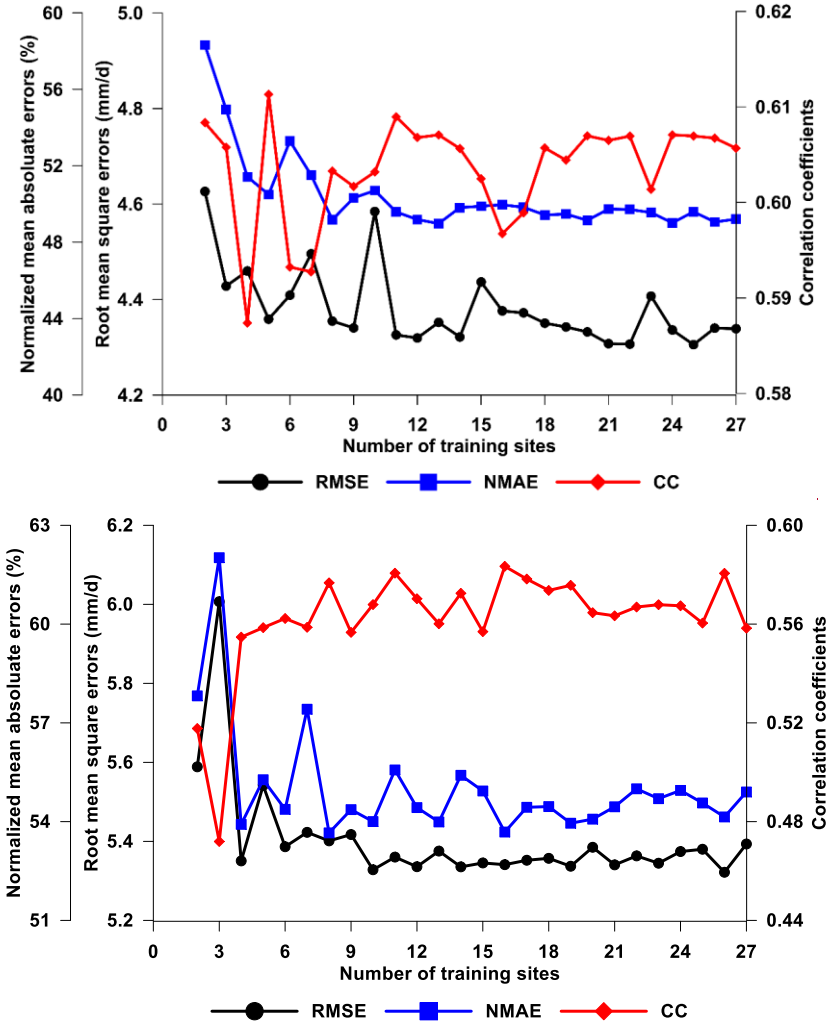

825 **Figure ~~14~~14:** Statistical error indices (i.e., RMSE, NMAE, and CC) of the blended SPE at the validation grid locations in terms of different number of training sites in the warm season of 2014 in the NETP.